Early alterations in the electrophysiological properties of rat spinal motoneurones following neonatal axotomy

George Z. Mentis[1,2], Eugenia Díaz[1], Linda B. Moran[1] and Roberto Navarrete[1]

[1]*Division of Neuroscience and Mental Health, Department of Cellular & Molecular Neuroscience, Imperial College London, Fulham Palace Road, London W6 8RF, UK*
[2]*Section of Developmental Neurobiology, Building 35, Room 3C1010, NINDS, NIH, Bethesda, MD 20892, USA*

Early in development, motoneurones are critically dependent on their target muscles for survival and differentiation. Previous studies have shown that neonatal axotomy causes massive motoneurone death and abnormal function in the surviving motoneurones. We have investigated the electrophysiological and morphological properties of motoneurones innervating the flexor tibialis anterior (TA) muscle during the first week after a neonatal axotomy, at a time when the motoneurones would be either in the process of degeneration or attempting to reinnervate their target muscles. We found that a large number (∼75%) of TA motoneurones died within 3 weeks after neonatal axotomy. Intracellular recordings revealed a marked increase in motoneurone excitability, as indicated by changes in passive and active membrane electrical properties. These changes were associated with a shift in the motoneurone firing pattern from a predominantly phasic pattern to a tonic pattern. Morphologically, the dendritic tree of the physiologically characterized axotomized cells was significantly reduced compared with age-matched normal motoneurones. These data demonstrate that motoneurone electrical properties are profoundly altered shortly after neonatal axotomy. In a subpopulation of the axotomized cells, abnormally high motoneurone excitability (input resistance significantly higher compared with control cells) was associated with a severe truncation of the dendritic arbor, suggesting that this excitability may represent an early electrophysiological correlate of motoneurone degeneration.

(Resubmitted 27 March 2007; accepted after revision 17 May 2007; first published online 17 May 2007)
Corresponding author G. Z. Mentis: Laboratory of Neural Control, Building 35, Room 3C1010, NINDS, NIH, Bethesda, MD 20892, USA. Email: mentisg@ninds.nih.gov

The effects of motoneurone (MN) disconnection from their targets are age dependent. Axotomy in adulthood results in temporary functional changes followed by almost complete recovery if reinnervation is allowed to occur. Unlike adult axotomy, neonatal axotomy results in cell death (Romanes, 1946; Schmalbruch, 1984; Lowrie *et al.* 1987), the extent of which depends upon the site and severity of axonal injury (Kashihara *et al.* 1987). The mechanisms involved in axotomy-induced MN death are not well understood, although the loss of trophic factors derived from muscles may be partly responsible (Wiese *et al.* 2004).

We have previously shown that following neonatal axotomy, those MNs that survive into adulthood and reinnervate fast ankle dorsiflexor muscles exhibit a shift in their firing pattern from phasic to tonic (Navarrete & Vrbová, 1984; Vejsada *et al.* 1991). Chronic electromyogram (EMG) recordings from the tibialis anterior (TA) muscle in freely moving rats revealed that the discharge pattern of the muscle was altered permanently after a neonatal sciatic nerve crush. No such change was observed in similar recordings obtained from the soleus muscle. In contrast, axotomy in the adult animal does not result in any changes in the firing pattern of motoneurones reinnervating either dorsiflexor or plantar extensor muscles (Navarrete & Vrbová, 1984).

Vejsada *et al.* (1991) also observed that the postural spinal reflexes of neonatally axotomized adult (reinnervated) TA motoneurones revealed significant abnormalities, which led them to suggest that the changes in flexor motoneurones may reflect increased motoneurone excitability. Additional evidence that neonatal axotomy results in a hyperexcitability of injured motoneurones comes from one of our previous studies in which we have reported that neonatally axotomized MNs may also be more vulnerable to excitatory glutamatergic synaptic drive and may eventually degenerate (Mentis *et al.* 1993).

To investigate the mechanisms that might be responsible for the altered firing pattern of TA motoneurones following

 DOI: 10.1113/jphysiol.2007.133488

neonatal axotomy, we compared the active and passive membrane properties and the firing behaviour of normal and axotomized TA motoneurones during the first week after nerve crush, by employing the isolated spinal cord–hindlimb preparation *in vitro*.

A second reason to investigate neonatal axotomy was to study possible mechanisms of cell death. Several lines of evidence implicate glutamate toxicity in this process. First, axotomy-induced cell death can be substantially reduced by application of glutamate antagonists after the axotomy (Mentis *et al.* 1993; Greensmith *et al.* 1994; Gougoulias *et al.* 2007). Second, axotomized motoneurones are known to be more susceptible to glutamate toxicity than normal motoneurones (Greensmith *et al.* 1995). Finally, after axotomy, there is a substantial upregulation of glutamate receptors on motoneurones (Virgo *et al.* 2000). After axotomy, adult motoneurones exhibit a transient increase in excitability. If such a change also accompanies neonatal axotomy, it might account for the extreme susceptibility of neonatal motoneurones to glutamate toxicity following axotomy. To investigate this possibility, we examined the intrinsic excitability of axotomized motoneurones and compared them to control MNs within the first week after axotomy, when many motoneurones die. Although we had no direct marker of cell death, we found that a subset of axotomized motoneurones exhibited a grossly abnormal morphology manifested by severe truncation of the dendritic arbor and extreme hyperexcitability consistent with degeneration.

Methods

Surgery

A total of one hundred and fifteen albino Sprague–Dawley rats of both sexes were used in this study. All surgical procedures were carried out in compliance with the UK Animal (Scientific Procedures) Act 1986. To study the time course of MN death, a total of 23 normal and 30 axotomized animals were used for retrograde labelling of motoneurones with fluorescent markers. Electrophysiological analysis was carried out in 32 normal (postnatal day, P3–P6, $n = 13$; and P7–P9, $n = 19$) and 30 axotomized animals (P3–P6, $n = 15$; and P7–P9, $n = 15$).

Newborn rats (P0) were anaesthetized with ether, and the TA muscles were injected bilaterally with 0.5 μl of an aqueous suspension of 2.5% Fast Blue (FB) and 2.5% Diamidino Yellow dihydrochloride (DY; EMS-Polyloy, Groβ-Umstadt, Germany). The FB labelled the soma and proximal dendrites and the DY labelled the nucleus of MNs. This labelling procedure was used to avoid double counting of MNs from serial sections. Two days later (P2), allowing time for retrograde transport of the dyes to the soma of TA MNs, the rats were re-anaesthetized, and the right common peroneal (CP) nerve was exposed and crushed about 1–2 mm from the entry point into the muscle (Fig. 1*A*).

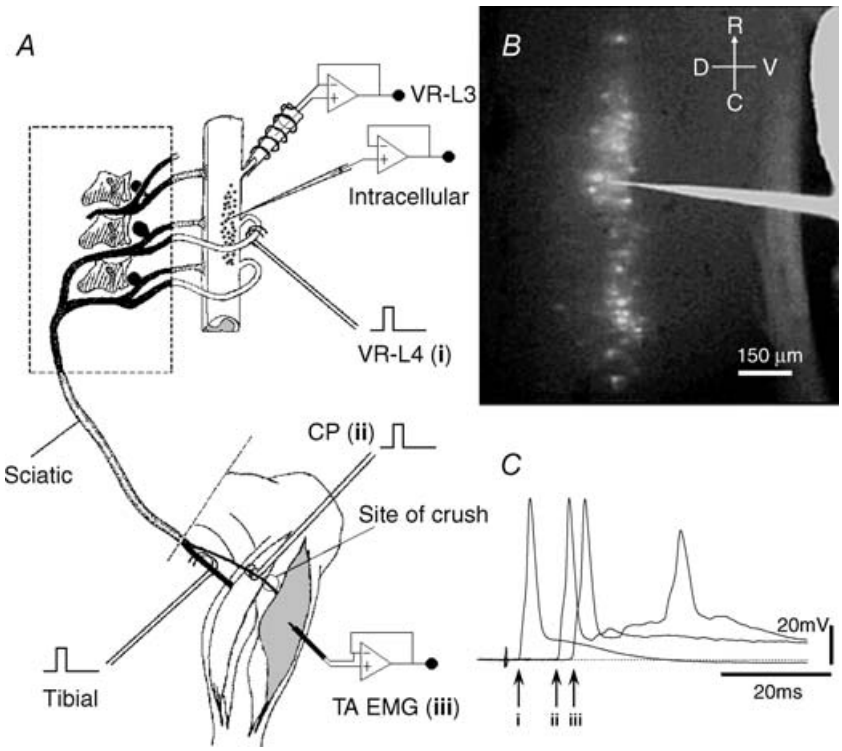

Figure 1. Experimental set-up
A, schematic representation of the hemisected spinal cord–hindlimb preparation. The tibialis anterior (TA) muscle was labelled on the day of birth (P0) with the fluorescent dyes Fast Blue and Diamidino Yellow (shaded muscle). Note the location of labelled TA motoneurone pool in the spinal cord (*A* and *B*). Recording and stimulating electrodes were placed in: (i) the ventral root (VR) L4; (ii) the common peroneal (CP) nerve proximal to the site of crush; and (iii) the TA muscle, to record the EMG and/or to stimulate. Synaptically mediated responses were assessed following stimulation of the peripheral nerves (tibial and common peroneal). The viability of the preparation was monitored from the VR-L3 recordings. *B* shows the extent of the retrogradely labelled TA motoneurone nucleus seen under epifluorescence and the intracellular microelectrode containing a mixture of Lucifer Yellow and neurobiotin (magnification ×10). R, rostral; C, caudal; V, ventral; and D, dorsal. *C*, superimposed traces recorded intracellularly in response to stimulation of: (i) VR-L4; (ii) CP nerve; and (iii) TA muscle (arrows indicate the onset of the antidromically evoked action potential).

Time course of axotomy-induced cell death

Motoneurone death was assessed by counting the number of FB/DY fluorescently labelled MN somata at various intervals after CP nerve crush (time points: P3, P5, P7, P14, P21 and 3 months old–adult). The animals were deeply anaesthetized (4% chloral hydrate, 2 ml (100 g body weight)$^{-1}$ I.P.) and perfused transcardially with 4% paraformaldehyde in 0.01 M phosphate buffer (0.027M KCl and 0.137M NaCl pH 7.4). The spinal cords were postfixed for at least 12 h and transverse serial sections (70 μm thick) were cut using a Vibratome (Series 1000, Vibratome, St. Louis, MO, USA). The somata of fluorescently labelled MNs were visualized using a Zeiss-Axioscope microscope equipped with an ultraviolet (UV) filter (365–420 nm excitation wavelength). Only MNs showing both cytoplasmic FB and nuclear DY labelling were counted. The results are expressed as the ratio of right/left side counts (see Fig. 2).

Hemisected spinal cord–hindlimb preparation

Intracellular recordings were carried out using the *in vitro* hemisected spinal cord–hindlimb preparation as described by Walton & Navarrete (1991). Rats were anaesthetised with ether and decapitated with a pair of sharp scissors. The dissection was performed under a continuous flow of cold (~4°C) oxygenated Krebs solution. The spinal cord was divided mid-sagitally, leaving the right hemisected spinal cord in continuity with the spinal roots and the hindlimb. The sciatic nerve and its two major branches, the common peroneal and tibial nerves, were identified and dissected free to facilitate placement of stimulating electrodes.

Electrophysiological recordings

Figure 1 shows a schematic drawing of the experimental set-up. The preparation was mounted on the stage of a purpose-built micromanipulation microscope equipped with Nikon optics and epifluorescence (M2B, Micro Instruments, Oxford, UK) and perfused at a rate of 3–5 ml min^{-1} with oxygenated Krebs solution maintained at room temperature (23–25°C). The Krebs solution consisted of (mM): 113 NaCl, 4.5 KCl, 1 Mg_2SO_4, 2 $CaCl_2$, 1 Na_2HPO_4, 25 $NaHCO_3$ and 11 glucose.

Extracellular electrodes were switched between recording and stimulation modes. Stimulation was performed using a stimulus-isolated constant-voltage unit (DS2, Digitimer, Letchworth Garden City UK). A suction electrode was used to record the ventral root potential from the third lumbar ventral root (VR-L3) in response to peripheral nerve stimulation, which allowed the viability of the preparation (Fig. 1*A*, VR-L3) to be monitored. Bipolar electrodes made from twisted Teflon-coated silver wires (Advent Research Materials Ltd, Eynsham, Oxford, UK) were used for stimulation of peripheral nerves (CP and tibial) or the VR-L4 (Fig. 1*A*). A concentric bipolar electrode (NE-100, Clark Electromedical Instruments, Reading, UK) was used to record the EMG and to stimulate intramuscular branches of the nerve supplying the TA muscle. Signals were differentially amplified using a Neurolog AC preamplifier (NL 104, Digitimer) filtered (NL 125, Digitimer) and fed to an analog-to-digital converter (1401 plus, CED, Cambridge, UK).

The retrogradely labelled TA motoneurone pool was visualized from the lateral aspect of the hemicord under epifluorescence illumination using long working distance objectives (Dekkers *et al.* 1994). The addition of Lucifer Yellow to the micropipette solution (Fig. 1*B*) facilitated targeting of individual MNs for intracellular recording. Images were captured using a CCD black/white video camera (WVBL-600, Panasonic, Japan) and stored in an IBM computer using commercially available software (RGB-Video, G2-Imaging, London, UK) for future reference.

Intracellular recordings were made in bridge mode using an Axoclamp 2B amplifier (Union Molecular Devices, Sunny vale, CA USA). Glass microelectrodes (GC120TF-10, 1.2 mm o.d., 0.94 mm i.d., Clark Electromedical Instruments) pulled using a Kopf 720 micropipette puller (D. Kopf Instruments, Tujunga, CA, USA) to a final resistance of 15–30 MΩ were used. The electrodes were filled with 1.5 M potassium acetate, 4% neurobiotin (Vector Laboratories) and 0.3% Lucifer Yellow CH (LY, Sigma). The recorded signals were stored in a personal computer using the SIGAVG software (CED) for off-line analysis.

Data acquisition and analysis

Motoneurones included for analysis fulfilled the following criteria: (i) stable resting potential of at least −55 mV; (ii) overshooting action potential; and (iii) recording time of at least 30 min. To ensure uniformity, electrophysiological properties were recorded at a holding membrane potential of −60 mV.

Antidromic action potentials were initially evoked by single-pulse stimulation (pulse duration: 0.2 ms) of the VR-L4 (or VR-L5), CP nerve and the TA muscle nerve. This method confirmed the identity of the MN, based on visual identification from the fluorescent signal in the soma. It was important to identify axotomized TA motoneurones, since an antidromic action potential could be elicited following stimulation of the CP nerve proximal to the site of injury but not from the TA muscle nerve. Stimulation of either the CP nerve or the TA muscle resulted in an antidromic spike followed closely by a synaptic response masking the after-depolarization (ADP) and after-hyperpolarization (AHP) of the spike. Therefore, we measured the ADP and AHP from action potentials evoked upon stimulation of the ventral root.

The following parameters associated with the VR-L4/5 antidromic action potential were measured:

Table 1. Membrane properties of normal and axotomized TA motoneurones

	Experimental groups			
Parameter	Normal (P3–P6)	Normal (P7–P9)	CP Crush (P3–P6)	CP Crush (P7–P9)
n	17	24	27	23
Resting potential (mV)	−66.88 ± 1.46	−63.30 ± 1.08	−65.16 ± 1.49	−64.38 ± 1.32
Spike amplitude (mV)	70.35 ± 2.32	69.64 ± 1.48	81.28 ± 2.09*†	79.90 ± 2.34*†
Spike overshoot (mV)	5.84 ± 1.64	7.48 ± 1.50	22.69 ± 1.92*†	17.91 ± 2.04*†
Spike half-width (ms)	1.67 ± 0.09	1.65 ± 0.07	1.45 ± 0.12	1.51 ± 0.08
Rate of rise (mV ms^{-1})	39.61 ± 3.58	41.03 ± 2.83	69.99 ± 5.30*†	59.30 ± 3.33*†
AHP amplitude (mV)	−1.82 ± 0.21	−1.46 ± 0.20	−3.15 ± 0.43*†	−3.26 ± 0.34*†
AHP duration (ms)	76.51 ± 6.99	68.00 ± 3.55	130.09 ± 7.14*†	129.71 ± 10.11*†
Input resistance (MΩ)	13.64 ± 2.10	6.22 ± 0.86*	19.67 ± 2.01†	19.40 ± 2.49†
Time constant (ms)	2.78 ± 0.44	2.40 ± 0.20	5.36 ± 0.62*†	4.79 ± 0.54*†
Rheobasic current (nA)	2.76 ± 0.59	3.33 ± 0.51	1.41 ± 0.18*†	1.21 ± 0.19*†
Voltage threshold (mV)	−45.0 ± 1.78	−47.31 ± 1.23	−44.28 ± 1.35	−46.03 ± 0.98

Statistical significance was calculated using two-way ANOVA. *$P < 0.05$ with respect to normal (P3–P6); †$P < 0.05$ with respect to normal (P7–P9). The results are expressed as means ± S.E.M.

(i) resting potential; (ii) spike amplitude; (iii) overshoot; (iv) time-to-peak amplitude; (v) spike duration at half-amplitude; (vi) threshold (voltage) of evoking an antidromic action potential; (vii) AHP amplitude; (viii) AHP duration; and (ix) presence/absence of ADP. The presence or absence of ADP was determined from a clear break in the repolarizing phase of the spike. If no break was observed and the repolarizing phase of the spike followed smoothly into the AHP, the ADP was considered to be absent (see Fig. 4). The duration of the AHP was measured from the falling phase of the action potential crossing the baseline, to the point at which the AHP membrane trajectory returned to the resting membrane potential. The threshold of membrane potential for evoking an antidromic action potential from ventral root stimulation was determined by three positive all-or-none responses out of five trials.

The passive membrane properties were assessed by injection of depolarizing and hyperpolarizing current pulses (100 ms duration) at the resting membrane potential. The input resistance (R_{in}) was calculated from the slope of the current–voltage plot within the linear range. The time constant was calculated as the time taken for the membrane potential to reach 66.7% of the steady-state voltage in response to a current step. The rheobasic current (I_{rh}) was determined as the depolarizing current required to evoke a single action potential. The action potential and passive membrane properties were measured from single traces, except for the AHP duration and AHP amplitude (shown in Table 1).

Repetitive firing properties were studied following injection of depolarizing current for 1 s. To characterize and compare quantitatively the firing patterns of normal and axotomized MNs, we calculated the instantaneous firing rate as the inverse of the interspike interval (ISI; expressed in Hz), at two different levels of current injection: (i) at the threshold (Thr) of current required for repetitive firing (minimal firing rate); and (ii) at twice the threshold current strength (2 × Thr). The latter was assigned arbitrarily as the maximal firing rate, although some MNs were capable of firing at higher frequencies. The minimal and maximal firing rates (expressed in Hz) were calculated as the inverse of the mean of ISIs from all steps of injected current (increments of 0.1 from Thr to 2 × Thr) for: (i) the first ISI; (ii) the first 100 ms; and (iii) the last 500 ms of current injection (adapted). The coefficient of variation (CV) was calculated as the standard deviation of the ISIs divided by the mean of the ISIs at the threshold for repetitive firing (minimal firing rate) and twice the threshold (2 × Thr; maximal firing rate).

For synaptically mediated responses, the CP and tibial nerves were stimulated. The threshold stimulus intensity which resulted in a consistent synaptic response was determined, and subsequent stimulus intensities were delivered at two to five times threshold. Unless otherwise indicated, recordings shown in this study are the averages of three to five individual events evoked at a stimulus frequency of 0.2 Hz. Stimulation at 0.2 Hz produced minimally depressed synaptic responses.

Morphology of intracellularly filled CP motoneurones

Following electrophysiological characterization, several MNs were intracellularly filled with neurobiotin. The tracer was injected by depolarizing steps of current (0.5–3.0 nA, 200 ms in duration at 3.3 Hz frequency) applied for 30 min and allowed to diffuse for at least another 30 min before the hemisected spinal cord was fixed in 4% paraformaldehyde. Visualization was achieved according to the procedure described by Horikawa & Armstrong (1988). Briefly, the hemisected spinal cord was cut into parasagittal sections (100 μm) using a Vibratome and collected in 0.1 M phosphate buffer. Motoneurone visualization was carried out on individual sections, using the ABC method (Vector Laboratories, Peterborough,

UK) with diaminobenzidine (DAB) as a chromogen, and then sections were dehydrated, cleared and permanently mounted.

Sections containing labelled MNs were photographed using an Olympus BH2 microscope equipped with a drawing tube. In addition, two-dimensional reconstruction of the MN dendritic tree was carried out from serial sections for 22 intracellularly filled cells (control, $n = 11$; CP crush, $n = 11$). For this purpose, all the sections containing dendrites were drawn, at a final magnification of $\times 750$, using an Olympus BH2 microscope equipped with a drawing tube. A complete representation of the MN dendritic tree was obtained by consecutive superimposition of these drawings. Morphometric analysis of the dendritic tree was carried out on camera lucida-reconstructed MNs by measuring the length of all the dendrites, using a digitizing tablet (Summagraphics), hence the total dendritic length (TDL) per MN was calculated. Although the measurements for the dendritic length of MNs were taken from serial sections, this is an underestimate of the whole dendritic length because reconstructions were only conducted in two dimensions.

Statistics

Results are presented in the text and figures as means ± S.E.M. To assess statistical differences between the control and axotomized groups, we performed two-way ANOVA, Paired Student's *t* test and the non-parametric Mann–Whitney *U* test (significance taken as $P < 0.05$) using the software packages SigmaStat v.32 (Jandel Scientific, Erkrath Germany) or STATISTICA v.6 (Statsoft, Tulsa, OK USA). Relationships between somatic area and input resistance, as well as total dendritic length and input resistance, were assessed using the Pearson product–moment correlation (r). Comparison of the coefficient r between normal and axotomized cells was performed using a difference test (Statistica v.6). The coefficient of variation (CV) for the firing pattern between normal and axotomized MNs was tested for normality using the Shapiro–Wilk *W* test. Since the data were normally distributed, an ANOVA on Ranks sum test was used to test statistical significance. The data of input resistance, soma area and total dendritic length presented and correlated in Fig. 10 were tested for normality using the Shapiro–Wilk *W* test and were found to be normally distributed.

Results

Time course of motoneurone death and reinnervation

To assess the time course of MN death following CP nerve crush at P2 we performed MN counts in individual animals at various time points following injury. Approximately 75% of injured MNs were lost during the first 2 weeks after nerve crush (Fig. 2). The maximal rate of cell death was observed during the first 5 days after nerve injury. Figure 2*C* shows the percentage ratio of MNs in the left and right sides of the spinal cord in normal animals and in those subjected to CP nerve crush on the right side. Counts of prelabelled TA MNs on both sides of the spinal cord in normal animals revealed that the fluorescent dyes *per se* did not have any significant effect on MN death (data not shown). There were on average 152.9 ± 6 TA MNs (average of left and right counts in 23 normal animals; 4 animals per time point except in adults where $n = 3$). No significant changes were observed in comparison with the number

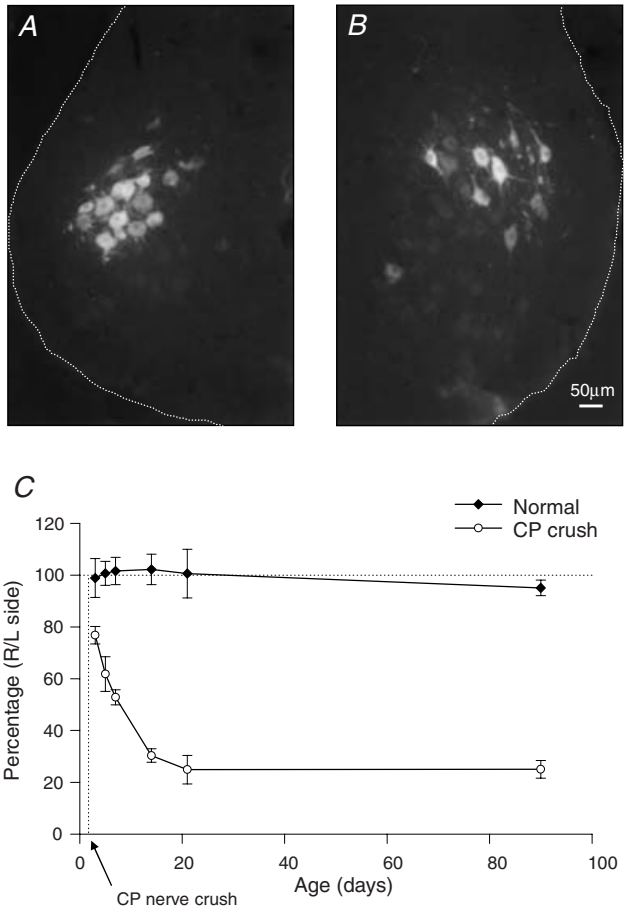

Figure 2. Time course of axotomy-induced motoneurone death
Transverse sections of a P7 spinal cord showing Fast Blue/Diamidino Yellow labelled TA motoneurones on the control (*A*) and injured side (*B*). There were fewer motoneurones labelled on the side of the nerve crush. Note the presence of small microglial-like cells within the axotomized motoneurone nucleus (*B*). *C*, TA motoneurone counts were expressed as a percentage of motoneurone number in the right side (nerve crush) divided by the number on the left (contralateral) side. Counts from normal (non-injured) animals (♦) revealed that there is no difference between the two sides of the spinal cord. In contrast, counts from injured animals (○) show that CP nerve crush at P2 results in ∼75% motoneurone death. The maximal rate of cell death was observed during the first 5 days after nerve injury.

of MNs on the contralateral (control) side of injured animals (157.7 ± 5.1; 30 injured animals; 5 animals per time point), consistent with previous reports (Peyronnard & Charron, 1983; Peyronnard *et al.* 1986). The ventral horn of the spinal cord from a P7 animal subjected to unilateral nerve crush is shown in Fig. 2*A* and *B*. On the control side (Fig. 2*A*), a group of fluorescently labelled TA MNs is seen in the dorsolateral part of the ventral horn. On the injured side (Fig. 2*B*), there were fewer labelled MNs, and a concomitant increase in the number of small fluorescently labelled microglial-like cells was seen. These cells may have taken up the fluorescent label by phagocytosis of dying MNs (Greensmith & Navarrete, 1994).

It has been proposed that successful reinnervation increases the chance of MN survival (Lowrie & Vrbová, 1992). In this study, we investigated the extent of reinnervation by stimulating the CP nerve proximal to the site of injury and recording the EMG responses from the TA muscle. We found that during the first 3 days after CP nerve crush (P3–P5), none of the preparations was reinnervated (0/9), whereas at P7–P9 about 30% of the preparations (2/7) of the injured spinal cords showed relatively small EMG responses to nerve stimulation indicative of early reinnervation. These results are in agreement with previous observations (Navarrete, 1991; Naidu *et al.* 1996). Although intracellularly recorded axotomized motoneurones were tested for reinnervation by the presence of an antidromic action potential in response to stimulation of the TA muscle nerve using the indwelling EMG electrode, none of the cells reported in this study could be activated antidromically from the muscle.

Electrophysiological characteristics

In order to investigate the electrophysiological characteristics of axotomized MNs shortly after nerve injury, at the time when the fate of MNs is unknown, we performed intracellular recordings from axotomized and control TA MNs during the first 7 days (P3–P9) after CP crush. Intracellular recordings were obtained from a total of 41 normal and 50 axotomized TA motoneurones that showed a stable membrane potential of at least -55 mV which could be maintained for at least 30 min in order to fully characterize the electrophysiological properties of these cells. Table 1 summarizes the electrophysiological parameters of normal and injured MNs in the two age groups studied (P3–6 and P7–9) and their statistical differences.

Since a depolarized resting potential may be a characteristic of degenerating MNs, we also compared a smaller set of normal and axotomized MNs which exhibited a resting potential more positive than -55 mV or which could not be recorded for as long as 30 min (i.e. cells that did not meet our criteria for analysis; see Methods). The mean ($\pm$ S.E.M.) resting potential in 7 normal TA MNs in the P3–6 age group was -48.7 ± 2.5 mV (recording time, 8 ± 1 min) and -50.1 ± 1.2 mV in 10 normal TA MNs in the P7–9 age group (recording time, 17 ± 7 min). The mean resting potential in axotomized TA MNs was not significantly different (two-way ANOVA) compared with normal MNs (CP crush P3–6 group -49.6 ± 2.3 mV, $n = 5$, recording time 11 ± 6 min; CP crush P7–9 group -47.3 ± 1.8 mV, $n = 9$, recording time 10 ± 5 min). The percentage of cells excluded on the basis of a depolarized resting potential or insufficient duration of recording was as follows: 41% (7/17) P3–6 control MNs; 42% (10/24) P7–9 control MNs; 19% (5/27) P3–6 axotomized MNs; and 39% (9/23) P7–9 axotomized MNs. These results therefore indicate that the depolarized resting potential present in some cells not used for the present analysis appears to be due to damage inflicted by the electrode impalement.

Action potential characteristics. The TA motoneurones were identified by the presence of: (i) fluorescent prelabel in the cell body; (ii) an antidromic action potential (AP) following stimulation of the VR-L4; (iii) an antidromic AP following stimulation of the CP nerve; and (iv) for control MNs only, also an antidromic AP following stimulation of the TA muscle-nerve (Fig. 1*C*). In both normal and axotomized MNs, the antidromic action potential evoked by the stimulation of the CP nerve was followed closely by synaptically mediated responses, which resulted in the 'masking' of ADP and AHP (Fig. 1*C*). Therefore, action potential parameters were analysed from the VR-L4 evoked antidromic action potential. In addition, to avoid possible interference owing to Renshaw inhibitory potentials, we averaged 10 spikes evoked by ventral root stimulation at high frequency (5 Hz).

The amplitude and duration of the AP remained largely unchanged in normal MNs during the developmental period studied (Fig. 3*D* and Table 1). However, comparison of the AP waveform between normal and injured MNs showed striking differences, as illustrated in Fig. 3. Injured MNs exhibited significantly larger amplitude and overshoot of the AP compared with normal (Fig. 3*A* and *B* and Table 1). The rising phase of the antidromic AP of normal MNs was characterized by a clear break between the initial segment and somatodendritic (IS-SD) components of the antidromic spike (Fig. 3*C*, arrow), as previously demonstrated for both adult and neonatal MNs (Brock *et al.* 1953; Fulton & Walton, 1986). In contrast, the vast majority of axotomized MNs did not show a clear IS-SD break. The presence of an IS-SD break is dependent on the membrane potential (Brock *et al.* 1953; Fulton & Walton, 1986) and is more prominent in hyperpolarized cells. However, since all measurements of electrophysiological parameters were carried out at a holding membrane potential of -60 mV, the loss of the IS-SD break of the AP is probably a consequence of nerve injury.

Associated with the loss of the IS-SD break, there was an increase in the rate of rise of the action potential in the injured MNs, which was already evident in the first 3 days after injury (Fig. 3*C* and *E* and Table 1). In contrast, the rate of repolarization was not appreciably altered (Fig. 3*C*). The mean duration of the action potential (at half-amplitude) was shorter in injured MNs but did not reach significant levels (Table 1).

After-depolarization and after-hyperpolarization. Alterations in active membrane properties following axotomy may lead to alterations in the firing pattern of the MN. We therefore analysed in detail two parameters of the AP, the ADP and the AHP, which are closely associated with the pattern of firing. In most normal neonatal TA motoneurones, the action potential was followed by a prominent ADP and a relatively short AHP (approximately 50–80 ms). The ADP could take the form of a depolarizing 'hump' (Fig. 4*A*, arrow) or follow smoothly the end of the repolarizing phase of the AP. Between 70 and 80% of normal TA MNs exhibited a 'hump-like' ADP (Fig. 4*C*). The presence of a prominent ADP was also associated with a particularly high incidence of 'doublet' firing, with the second spike riding on the ADP (Fig. 4*B* and *D*; Navarrete & Walton, 1989; Viana *et al.* 1993*a*; Martin-Caraballo & Greer, 2001). In contrast, this 'hump-like' ADP was conspicuously absent in the majority of axotomized MNs (Fig. 4*A* and *C*). At P3–P6, only 43.5% (10/23) of axotomized MNs exhibited an ADP and at P7–P9 this decreased further to 11.8% (2/17, see Fig. 4*C*). The loss of the ADP in the axotomized MNs was also correlated with a marked decrease in the incidence of doublet firing which was already evident within the first few days after injury (Fig. 4*D*).

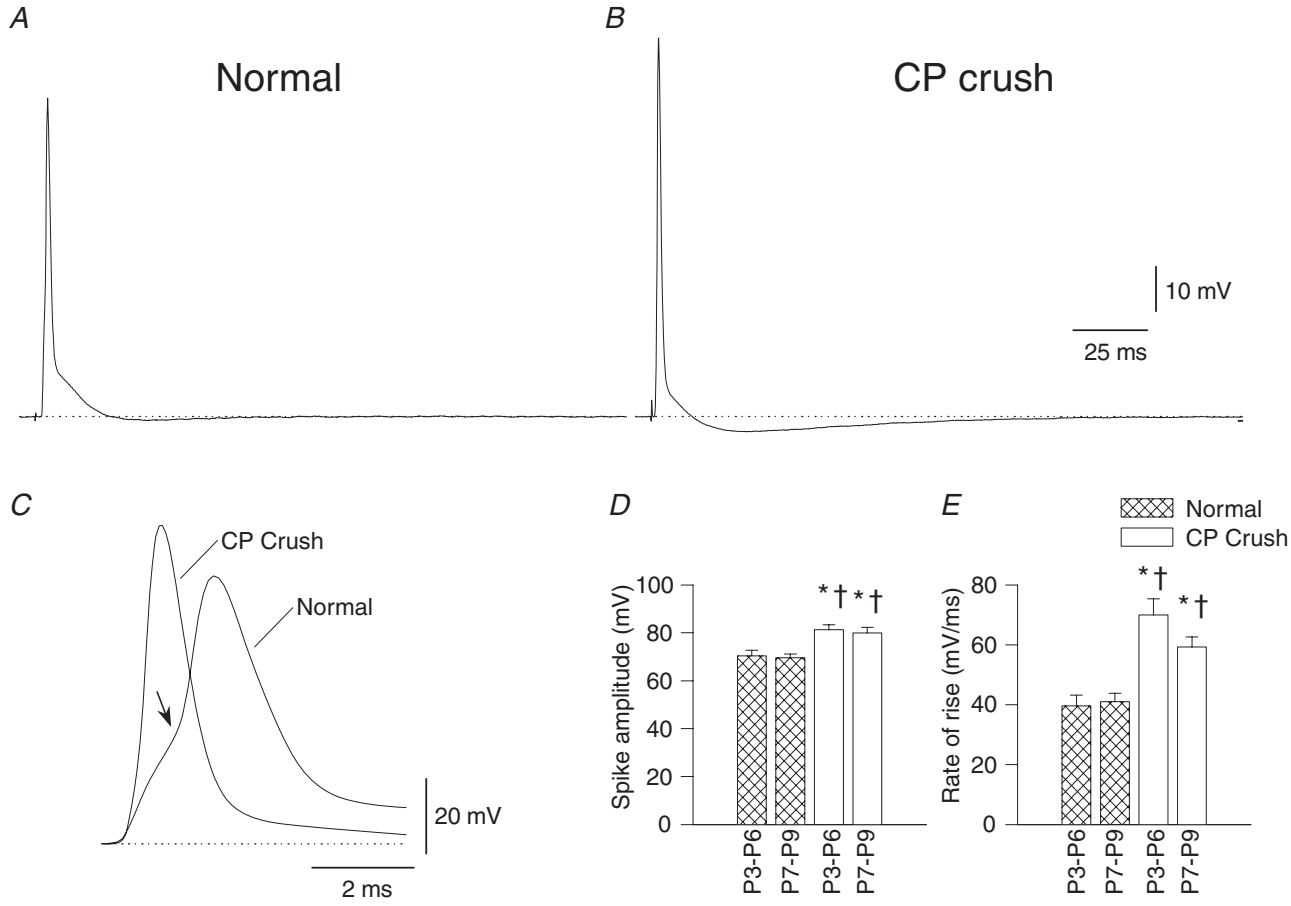

Figure 3. Altered action potential characteristics following neonatal axotomy
Antidromic action potentials elicited by ventral root L4 stimulation in a P8 normal (*A*) and a P7 injured TA motoneurone (*B*). The two traces are superimposed and shown in (*C*) on an expanded time scale. The rising phase of the action potential in the normal cell shows a distinct initial segment-somatodendritic break (arrow), while this is absent in the injured cell. Note the larger amplitude and faster rate of rise of the action potential in the axotomized motoneurone. Note also the more pronounced after-hyperpolarization in the axotomized motoneurone. The resting potential in the normal and injured motoneurone was −60.5 and −61.7 mV, respectively. Comparisons of mean values of spike amplitude and rate of rise of the action potential are shown in *D* and *E*, respectively (*$P < 0.05$ compared with P3–P6 normal; †$P < 0.05$ compared with P7–P9 normal; two-way ANOVA).

In normal TA motoneurones at P3–P6, the amplitude and duration of the AHP was relatively short and there were no significant differences in either of these two parameters during early postnatal development (Fig. 5 and Table 1). However, injured MNs exhibited a larger and longer AHP at both ages studied (Fig. 5*B* and *C*). Comparison of the mean AHP between normal and injured MNs showed a significant twofold increase in the AHP amplitude and duration (Table 1). The plot of the distribution of AHP duration for the two populations of MNs at P7–P9 (Fig. 5*D*) revealed that approximately 40% of the injured MNs possessed AHPs with abnormally long duration, which was longer than the maximal value measured in the normal cells (> 110 ms). Finally, in order to test the possibility that the AHP duration may be affected as a result of changes in recurrent inhibition as a result of the axotomy *per se*, we compared the AHP duration in control and axotomized MNs following two different methods. The AHP duration was also measured for a smaller set of control and axotomized MNs after an action potential was evoked by small positive current injection and was measured by a similar method to the ventral root antidromic stimulation. The AHP duration was not significantly different between the two methods of measurements between control and axotomized MNs for any of the age groups. In particular, the AHP duration for three control MNs (age, P3–P6) following ventral root stimulation was 92.9 ± 21.9 ms, whereas for the same three MNs the AHP duration following orthodromic stimulation was 91.7 ± 12.8 ms (n.s.; paired Student's *t* test). Similarly, in three P7–P9 control MNs, it was 62.8 ± 8.2 ms (ventral root stimulation method), whereas following orthodromic stimulation it was 49.5 ± 4.2 ms (n.s.; paired Student's *t* test). The AHP duration in four

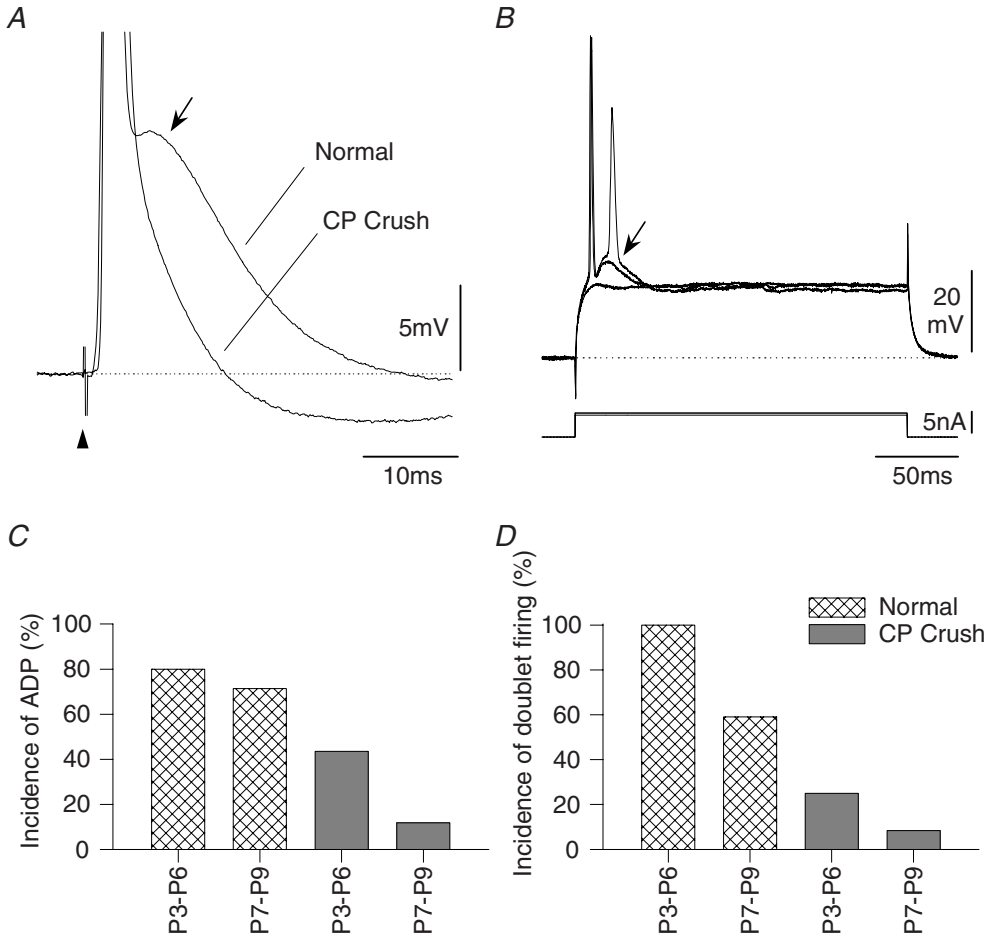

Figure 4. Reduction of after-depolarization (ADP) in injured motoneurones
A, superimposed traces of antidromically evoked action potentials (APs) from P7 normal and injured motoneurones, showing the presence of a prominent ADP in the normal motoneurone (arrow) and its absence in the injured cell. Arrowhead indicates the stimulus artifact. *B*, superimposed traces of orthodromically evoked APs following intracellular current injection (bottom traces) in a P6 normal cell. A second action potential was elicited at the peak of the ADP (arrow; normal resting potential, −62.4 mV and injured resting potential, −69.7 mV in *A*; and normal resting potential, −60.5 mV in *B*). Note the lower incidence of ADP (*C*) and doublet firing (*D*) in the injured motoneurones (population statistics).

P3–P6 axotomized MNs was 121.5 ± 19.6 ms (ventral root stimulation method), whereas following orthodromic stimulation it was 130.4 ± 14.7 ms (n.s.; Mann–Whitney *U* test). Finally, in the P7–P9 age group of axotomized MNs, the AHP duration for four MNs following ventral root stimulation was 150.7 ± 28.0 ms, whereas the AHP duration for the same four MNs following orthodromic stimulation was 170.8 ± 9.3 ms (n.s.; paired Student's *t* test).

Passive membrane properties. In order to further characterize the changes in membrane excitability of MNs following axotomy, we investigated the passive membrane properties in control and axotomized MNs. Figure 6 shows membrane voltage responses to hyperpolarizing and depolarizing current pulses for a normal and an injured MN. The input resistance (R_{in}) was calculated from the slope of the *I–V* plot (Fig. 6*C*). In normal MNs, there was a significant developmental reduction in input resistance and time constant between the two age groups (Fig. 6*E* and Table 1), indicating a developmental decrease in cell excitability. During the same period, the rheobasic current increased, although not significantly (Fig. 6*F* and Table 1).

Following neonatal nerve injury, the mean input resistance was significantly greater than control values for the two age groups studied (Fig. 6*E*, Table 1). The distribution of R_{in} values for P7–P9 control and axotomized MNs (Fig. 6*D*) reveals that approximately 45% of axotomized neurones have abnormally high values of R_{in}, ranging between 20 and 50 MΩ, well in excess of the highest value recorded from normal MNs. Similarly, a twofold increase in the time constant of axotomized MNs was observed (Table 1). Moreover, a significant reduction in the rheobasic current was observed in axotomized MNs with respect to age-matched controls (Fig. 6*F* and

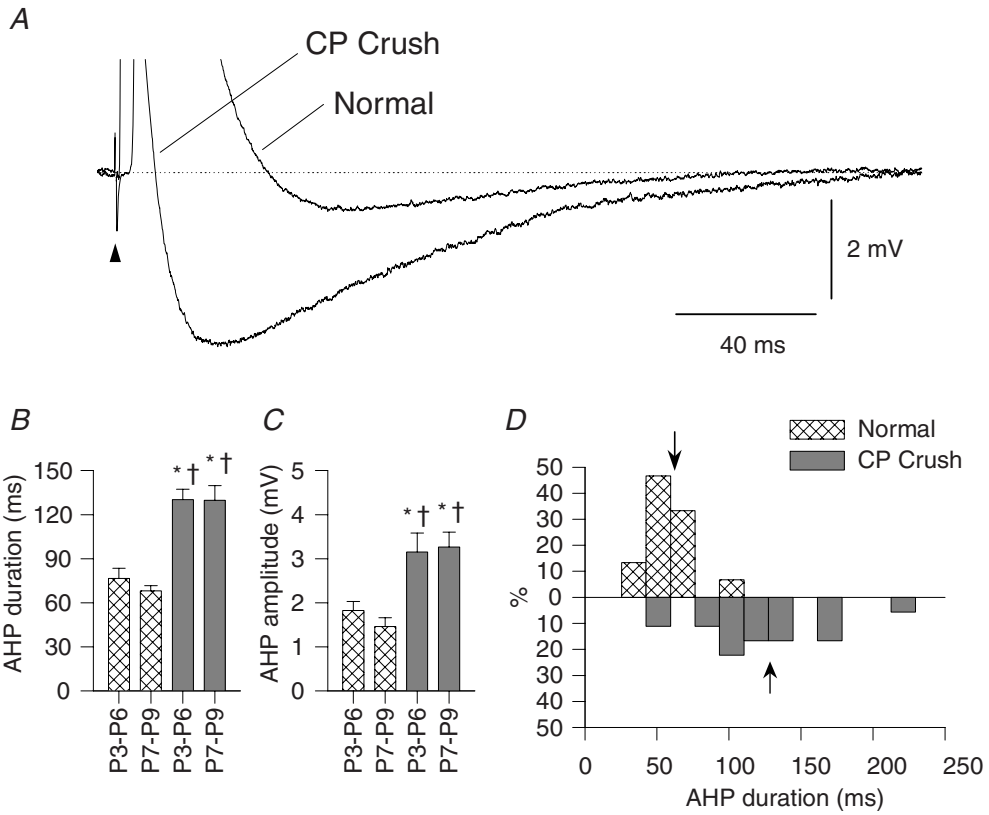

Figure 5. Increase of after-hyperpolarization after injury
A, superimposed traces of action potentials from P7 normal and injured motoneurones, showing the after-hyperpolarization. The injured motoneurone revealed a larger amplitude and longer duration after-hyperpolarization. The traces are averages of five consecutive responses acquired following VR-L4 stimulation at 1 Hz. The resting membrane potential was similar for both the normal (−63 mV) and the injured motoneurones (−65 mV). Arrowhead indicates the stimulus artifact. Comparison of the means for the AHP duration (*B*) and AHP amplitude (*C*) revealed significant differences between the groups early after CP nerve crush (*$P < 0.05$ compared with P3–P6 normal; †$P < 0.05$ compared with P7–P9 normal; two-way ANOVA). *D* shows the distribution of AHP duration for the population of motoneurones sampled in the P7–P9 age group. In approximately 45% of injured motoneurones the AHP duration was greater than the largest value in the normal group. Arrows indicate the mean value for each group.

Table 1). Since no significant differences were observed between normal and axotomized MNs with respect to the voltage threshold at which an action potential was evoked (Table 1), these changes demonstrate that there is a marked increase in MN excitability following neonatal axotomy.

Repetitive firing. The above-mentioned changes in passive and active membrane properties following nerve injury indicate that cells become more excitable after neonatal axotomy, a finding that should have implications for the MN firing behaviour. We therefore studied the repetitive firing pattern following long depolarizing current pulses (1 s) in 21 normal ($n = 9$ at P3–P6; $n = 12$ at P7–P9) and 17 injured TA motoneurones ($n = 8$ at P3–P6; $n = 9$ at P7–P9). The TA motoneurones exhibited four different types of firing pattern, as follows: (i) single action potential firing, which was independent of the amplitude of the depolarizing pulse (Fig. 7*A*); (ii) burst

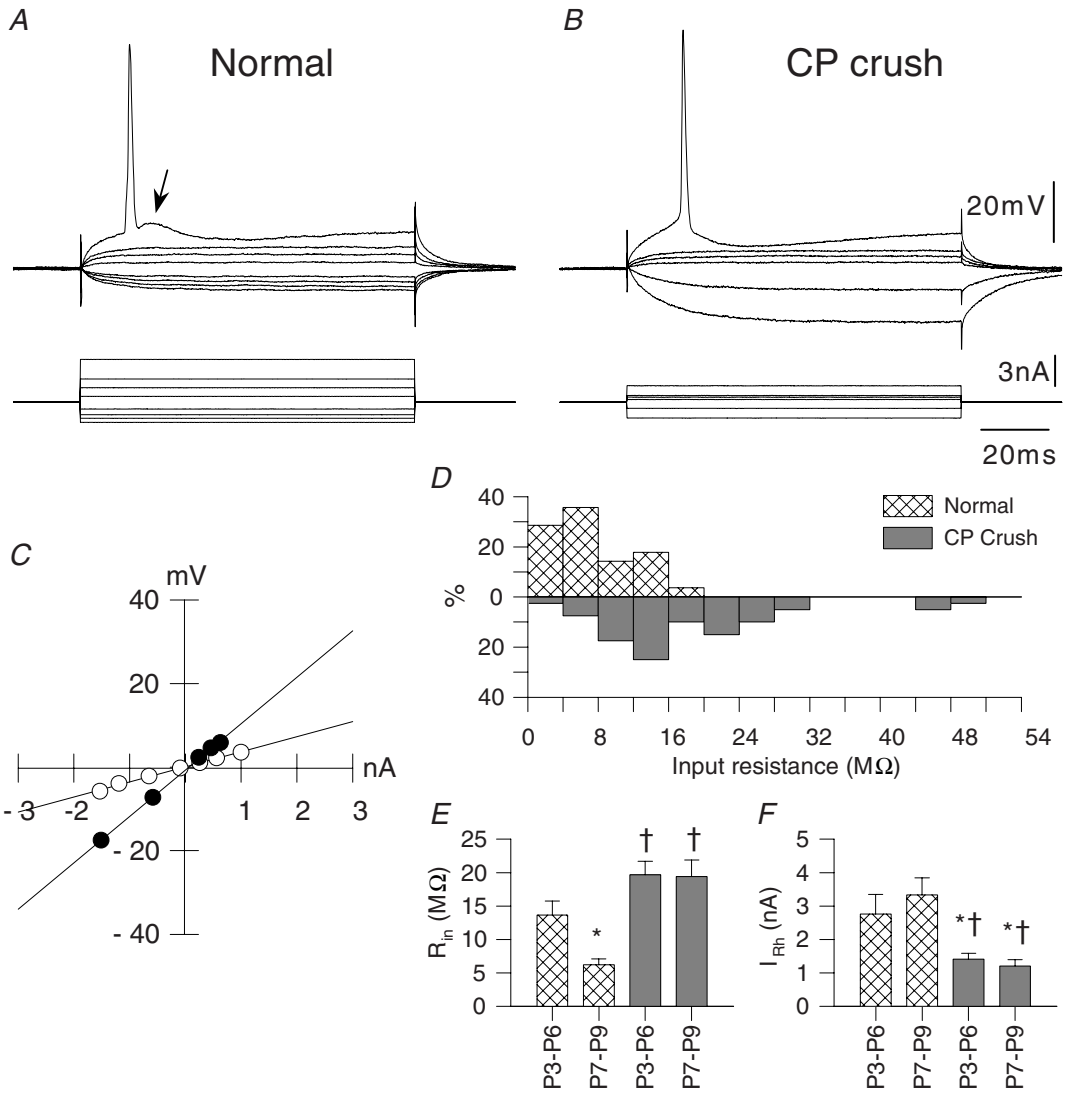

Figure 6. Passive membrane properties reveal an increased excitability in axotomized motoneurones
Superimposed traces of membrane potential in a P7 normal (*A*) and a P6 injured TA motoneurone (*B*) following depolarizing and hyperpolarizing current injections (bottom traces). Arrow in *A* indicates the presence of an after-depolarizing potential in the normal cell, which is absent in the axotomized motoneurone. The resting potential was −61.6 mV in the normal and −61.9 mV in the injured motoneurone. *C* shows the current–voltage relationship for the corresponding cells. The input resistance (calculated from the slope of the plot) was higher in the injured motoneurone (11.1 MΩ, ●) compared with the normal MN (3.6 MΩ, ○). *D* shows the distribution of the input resistance values in the population of motoneurones studied in the P7–P9 age group. Approximately 30% of injured motoneurones possessed abnormally high values, ranging between 20 and 50 MΩ. Injured motoneurones revealed on average a significantly higher mean of input resistance (*E*) and concomitantly, significantly lower mean for rheobasic current (*F*) compared with normal motoneurones in the two age groups (*$P < 0.05$ compared with P3–P6 normal; †$P < 0.05$ compared with P7–P9 normal; two-way ANOVA).

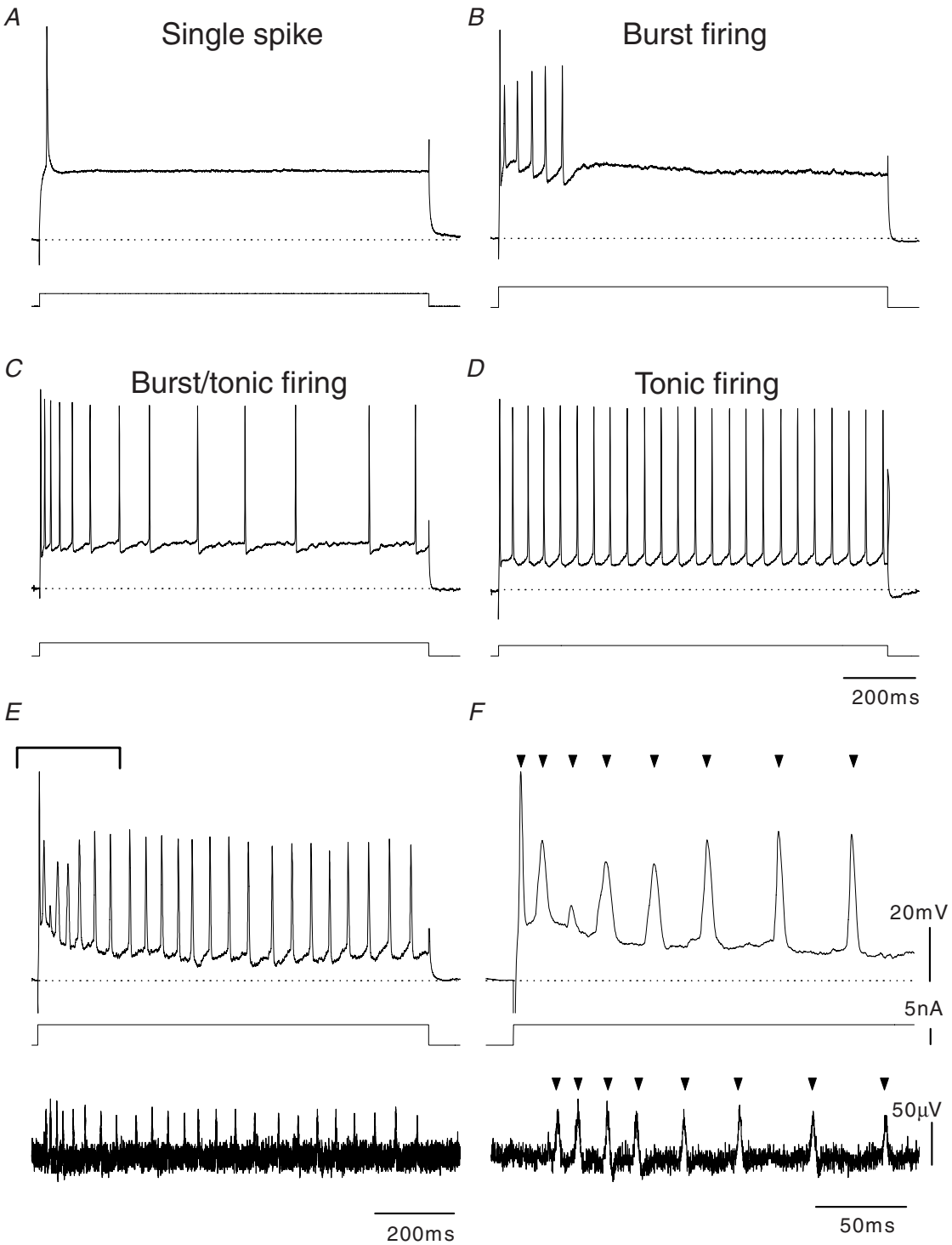

Figure 7. Firing patterns in normal motoneurones
Normal TA motoneurones exhibited four different patterns of firing (*A*–*D*) in response to suprathreshold depolarizing current pulses. *A* shows a P6 motoneurone which fired a single spike, independent of the intensity of current injection (resting potential, −71.3 mV). *B*, P8 motoneurone showed phasic (burst) firing only for the first 200 ms of the current pulse (resting potential, −68.1 mV). *C*, another P8 motoneurone, showing adapted (burst/tonic) firing (resting potential, −62.3 mV). *D*, a different P8 motoneurone firing tonically (resting potential, −68.9 mV; current pulses are shown in the bottom traces). In all cases, firing was evoked from the resting membrane potential. *E*, simultaneous recordings of the membrane response and EMG activity from the TA muscle following a depolarizing current pulse. *F* shows the first 200 ms in *G* on an expanded time scale. Note that each action potential elicited a motor unit potential (MUP) in the TA muscle (arrowheads), indicating that the motoneurone firing pattern is faithfully transmitted to the muscle.

firing, characterized by a phasic discharge of two or more action potentials, occurring within the first 200 ms of the beginning of the depolarizing pulse followed by quiescence (Fig. 7*B*); (iii) burst/tonic discharge, which was characterized by an initial burst for the first 100–200 ms followed by irregular sustained firing for the rest of the current pulse duration (Fig. 7*C*); and (iv) tonic firing, a continuous sustained firing with regular interspike intervals (ISI) throughout the depolarization (Fig. 7*D*).

It is worth noting that Vinay *et al.* (2000) found no relationship between input resistance and firing behaviour in a population of flexor motoneurones (antidromically identified from the common peroneal nerve) in the neonatal (P0–P2) rat. Specifically, they found that motoneurones unable to fire repetitively had similar input resistances to those exhibiting a maintained discharge in response to a step of current injection (26.4 ± 3.3 *versus* 28.8 ± 2.7 MΩ, respectively). Similarly, in our study, the membrane potential and input resistance were similar between the cells that fired repetitively and those that did not. Thus, methodological factors, such as damage resulting from electrode impalement, are not responsible for the different patterns observed. These may represent successive stages in the development of repetitive firing instead, as has been proposed by Vinay *et al.* (2000). In addition, cells in which an impalement artifact was suspected or where electrode rectification was observed were excluded from the analysis.

To provide a quantitative measure of the differences in the discharge patterns of normal and axotomized MNs, the rate and variability of firing were calculated at the beginning and end of the spike train, and the results are presented in Table 2. The majority of normal MNs exhibited a burst/tonic firing [P3–P6, 66.7% (6/9); P7–P9, 58.3% (7/12)] characterized by a relatively high rate of firing during the first 100 ms and a lower rate of adapted firing during the last 500 ms of the current injection pulse. In these cells, the CV of the ISI was high. At both ages, about 10% of the cells (P3–P6, 11.1%; P7–P9, 8.3%) exhibited a burst pattern of firing, in which firing could not be maintained for the whole duration of the current injection pulse. These cells showed a high instantaneous firing rate during the first 100 ms. Finally, a tonic pattern of firing was seen in only 16.7% (2/12) of the P7–P9 normal cells (no cells showed regular tonic firing in the normal P3–P6 group). About 20% of normal MNs (P3–P6, 22.2%; P7–P9, 16.7%) at both ages studied fired a single spike. These cells could not fire repetitively even with current pulses of more than twice the current threshold.

In many control preparations, during repetitive firing elicited by intracellular current injection, a small but distinct motor unit potential (MUP) was recorded from the TA muscle by the indwelling EMG electrode (Fig. 7*E* and *F*). The MUP consistently reproduced the firing pattern recorded intracellularly from the MN. The temporal correspondence between the two spike trains, and the fact that the amplitude of the MUP varied relatively little over time, suggest that the safety factor for neuromuscular transmission is sufficiently high for the MN firing pattern to be transmitted to the muscle.

Neonatal nerve injury induced a marked shift in the firing pattern of the TA motoneurones (Fig. 8 and Table 2). In contrast to normal MNs, in which the predominant pattern of firing was burst or burst/tonic, the vast majority of axotomized MNs exhibited a tonic firing pattern [P3–P6, 100% (8/8); P7–P9, 88.9% (8/9)]. Only one of the axotomized MNs in the P7–P9 age group (11.1%) exhibited burst/tonic firing and none could be classified into 'single spike' or 'burst' categories. Tonically firing cells were characterized by a regular interspike interval and a lower coefficient of variation of the ISI compared with burst/tonic MNs (Table 2). At the threshold for repetitive firing, there were significant differences in CV of the interspike interval between normal (49.9 ± 15.7 in P3–P6, 51.2 ± 14.5 in P7–P9) and injured MNs (13.6 ± 1.9 in P3–P6, 16.3 ± 2.1 in P7–P9; ANOVA on Ranks sum test). This difference is also evident in the frequency–current (*f–I*) relationship (Fig. 8*E* and *F*). Normal cells, stimulated at intensities close to threshold, exhibited a clear 'jump' in the firing frequency for the first and the second ISI (Fig. 8*E*), which is indicative of burst firing. In contrast, injured MNs exhibited a linear relationship between the firing rate and the intensity of current injection.

The coefficient of variation of the ISI at the threshold and twice the threshold of current required for repetitive firing in normal and injured MNs is shown in Table 2. None of the axotomized cells exhibited burst/tonic firing in the P3–P6 age group and only one exhibited this type of firing at P7–P9. The vast majority of axotomized cells in both age groups (16/17) displayed a tonic pattern of firing, whereas only two normal MNs in both age groups (2/21) exhibited tonic firing (Table 2). These results therefore demonstrate that peripheral nerve injury during early postnatal development leads to a marked shift of the firing pattern of TA motoneurones from a phasic or burst pattern typical of motoneurones innervating fast muscles towards a tonic firing pattern characteristic of MNs innervating slow muscles. This result suggests that neonatal axotomy results in permanent changes in MNs that survive into adulthood and have been shown to exhibit altered activity pattern (Navarrete & Vrbova, 1984).

Synaptic responses. To investigate possible alterations in the synaptic drive to axotomized MNs during the period when the vast majority of cells are disconnected from their target muscle, we assessed the synaptic responses following stimulation of dorsal roots and peripheral nerves. Tibialis anterior MNs receive depolarizing synaptic inputs

Table 2. Altered firing patterns of normal and axotomized TA motoneurones

			Experimental groups			
Firing pattern	Parameter		Normal (P3–P6)	Normal (P7–P9)	CP Crush (P3–P6)	CP Crush (P7–P9)
Total cells	*n* (number of cells)		9	12	8	9
Single Spike	*n*		2/9	2/12	0	0
Burst	*n*		1/9	1/12	0	0
	Max. firing rate (Hz)	First ISI	142.8	108.7	—	—
		First 100 ms	76.9	76.3	—	—
		Adapted	—	—	—	—
	Min. firing rate (Hz)	First ISI	91.0	65.8	—	—
		First 100 ms	19.2	32.8	—	—
		Adapted	—	—	—	—
Burst/tonic	*n*		6/9	7/12	0	1/9
	Max. firing rate (Hz)	First ISI	95.1 ± 24.3	107.6 ± 9.3	—	92.6
		First 100 ms	43.7 ± 7.3	58.8 ± 4.5	—	59.2
		Adapted	31.7 ± 8.5	26.9 ± 4.4	—	30.3
		CV (max. firing rate)	23.9 ± 0.4	28.3 ± 9.4	—	—
	Min. firing rate (Hz)	First ISI	43.9 ± 24.9	25.1 ± 10.9	—	35.2
		First 100 ms	20.0 ± 6.7	9.7 ± 3.4	—	20.2
		Adapted	12.2 ± 5.1	6.4 ± 2.2	—	7.1
		CV (min. firing rate)	49.9 ± 15.7	51.2 ± 14.5	—	—
	$I_{thr(RF)}$ (nA)		0.8 ± 0.2	2.8 ± 0.7	—	0.9
Tonic	*n*		0	2/12	8/8	8/9
	Max. firing rate (Hz)	First ISI	—	41.8	47.8 ± 14.6	67.7 ± 10.5
		First 100 ms	—	31.3	29.9 ± 4.1	36.1 ± 2.9
		Adapted	—	23.9	22.1 ± 1.7	20.6 ± 2.5
		CV (max. firing rate)	—	—	12.1 ± 2.6	17.6 ± 2.9
	Min. firing rate (Hz)	First ISI	—	26.2	13.2 ± 1.9	13.8 ± 1.3
		First 100 ms	—	19.1	12.1 ± 1.4	10.1 ± 0.6
		Adapted	—	13.4	9.6 ± 0.7	5.9 ± 0.9
		CV (min. firing rate)	—	—	13.6 ± 1.9	16.3 ± 2.0
	$I_{thr(RF)}$ (nA)		—	2.3	0.8 ± 0.1	1.5 ± 0.4

The TA motoneurones fired in four distinct firing patterns (single spike, burst, burst/tonic and tonic) in response to depolarizing current injections. Normal TA motoneurones exhibited mostly a burst/tonic firing, whereas axotomized TA motoneurones for the most part fired tonically. The minimal firing rate was calculated at the threshold for repetitive firing and the maximal firing rate was calculated at twice the threshold for repetitive firing. CV is the coefficient of variation and $I_{thr(RF)}$ is the minimal current required for the cells to fire repetitively for the whole duration of the current injection (1 s). The results are expressed as means ± S.E.M. when $n > 3$.

from the homonymous (common peroneal) nerve as well as the antagonistic (tibial) nerve. These synaptic inputs are mostly mediated via glutamatergic pathways originating from primary afferents (Kudo & Yamada, 1987; Pinco & Lev-Tov, 1993) and via glutamatergic/glycinergic/GABAergic pathways from interneurones. Stimulation of the CP nerve or tibial nerve at increasing intensity resulted in graded, short- and long-latency synaptic responses in both normal and injured preparations (Fig. 9). As previously shown (Ziskind-Conhaim, 1990; Pinco & Lev-Tov, 1993), both mono- and polysynaptic responses were reduced in amplitude by the NMDA receptor antagonist DL-2-amino-5-phosphonovaleric acid (APV) and were almost completely abolished by the non-NMDA receptor antagonist 6-cyano-7-nitroquinoxaline-2,3-dione (CNQX; data not shown). In normal preparations, stimulation of the CP nerve at twice threshold elicited an antidromic action potential followed by a sharp, short-latency monosynaptic response, which decayed rapidly towards the baseline (Fig. 9*A*). At higher stimulus intensities (5 × Thr), the monosynaptic response was followed by long-latency, asynchronous polysynaptic responses (Fig. 9*A*). Stimulation of the tibial nerve at both stimulus intensities elicited short- and long-latency synaptic potentials. The earliest potential evoked from the antagonist nerve had a short latency similar to that of the homonymous monosynaptic response and may therefore correspond to mono- or oligosynaptic potentials not normally found in mature animals (Seebach & Ziskind-Conhaim, 1994). Axotomized preparations exhibited very robust synaptic responses following stimulation of either CP or tibial nerve (Fig. 9*B* and *D*). Low-intensity stimulation of the CP nerve evoked a small short-latency monosynaptic potential at a comparatively longer latency than that of the normal animals (Fig. 9*B*). This could be attributed to a reduction in the conduction velocity of afferent fibres in the

injured CP nerve. At higher intensities of stimulation ($5 \times$ Thr), long-lasting synaptic potentials giving rise to repetitive firing were observed. Similar enhanced synaptic responses were observed in response to low- and high-intensity stimulation of the uninjured tibial nerve (Fig. 9*D*). Although a detailed analysis was not performed, one possible explanation for the apparently enhanced synaptic response observed in axotomized MNs could be their greater intrinsic membrane excitability. This enhanced synaptic activation of axotomized MNs raises the

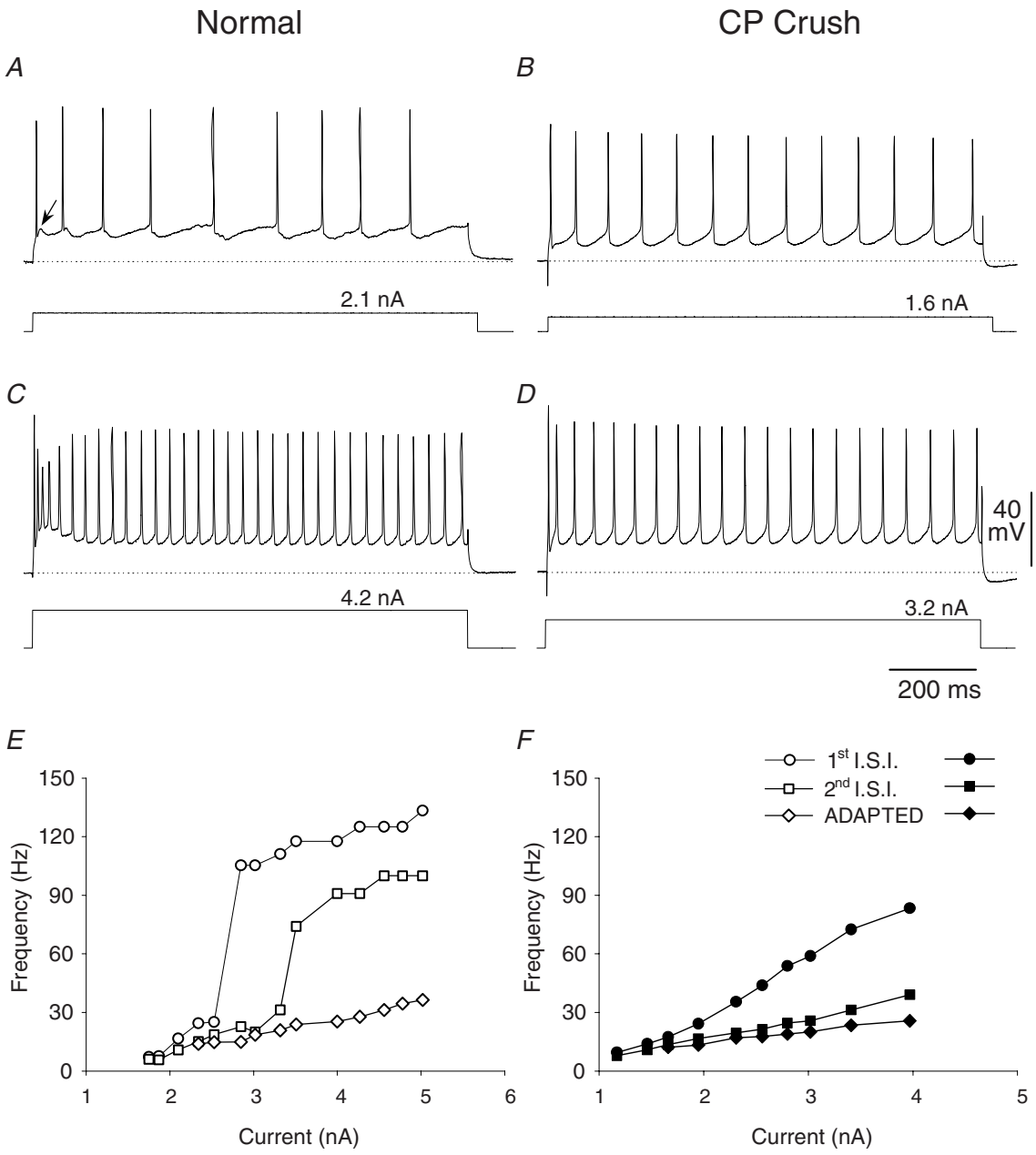

Figure 8. Switch from a phasic to a tonic firing pattern after neonatal axotomy
Intracellular responses of a P8 normal (*A* and *C*) and a P7 axotomized motoneurone (*B* and *D*) at two levels of depolarizing current injection. *A* and *B* are responses at the threshold for repetitive firing, and *C* and *D* are responses at twice the threshold for repetitive firing. Note that the normal motoneurone shows accommodation at the threshold for repetitive firing (*A*), in contrast to the axotomized motoneurone (*B*). At larger depolarizing current injection, the normal motoneurone elicited a burst type of firing at the onset of the spike train, which is due to the presence of the pronounced ADP (arrow in *A*). The resting membrane potential in the normal and axotomized motoneurones was −57.8 and −60.6 mV, respectively. *E* and *F* show the frequency–current relationship for the same normal and axotomized motoneurones. The values for the first two interspike intervals (ISI) and the adapted pattern are plotted.

possibility that glutamate-mediated excitotoxicity may be involved in neonatal axotomy-induced cell death (Mentis *et al.* 1993).

Changes in the morphological characteristics of motoneurones following nerve crush

In order to correlate the MN electrophysiological properties described above with morphometric parameters associated with the somatodendritic morphology of normal and axotomized MNs, some of the electrophysiologically characterized cells were intracellularly injected with neurobiotin and their dendritic tree was fully reconstructed at the light microscopy level using a camera lucida. Figure 10 shows camera lucida reconstructions of the dendritic tree of a normal (Fig. 10*A* and *B*) and two injured TA motoneurones (Fig. 10*C*–*F*). The mean somatic area of the injured MNs was smaller compared with that of age-matched controls, though the difference was not statistically significant (control, $609.7 \pm 56.6\ \mu m^2$, $n = 11$; CP crush, $516.9 \pm 39.7\ \mu m^2$, $n = 13$). Normal MNs possessed elaborate dendritic arborizations giving rise to complex branching patterns (Fig. 10*B*). The dendritic tree of injured MNs exhibited a range of morphologies, with some cells appearing qualitatively similar to normal MNs and others showing abnormal features, such as dendritic sprouting (data not shown, see Dekkers & Navarrete, 1998), or features reminiscent of neurodegeneration, such as swollen or beaded primary dendrites. The most notable difference was reduction of the size and complexity of the dendritic tree in injured MNs. Figure 10*C* and *D* shows that the injured MN has fewer branching points and some dendrites were unbranched (Fig. 10*C*, arrows). In two cases (2/11), injured TA motoneurones that were electrophysiologically characterized displayed a severely reduced dendritic tree that was consistent with advanced stages of neurodegeneration (Fig. 10*E* and *F*). Quantitative comparison of the total dendritic length (TDL) indicated a highly significant reduction in the dendritic tree in injured MNs (TDL of control, $10379.7 \pm 1099.8\ \mu m$, $n = 11$; TDL following CP crush, $4718.3 \pm 742.3\ \mu m$, $n = 11$; $P < 0.001$, paired Student's *t* test; Fig. 10*C* and *E*).

Figure 10*G* and *H* illustrates the correlation between electrophysiological and morphological parameters in the subpopulation of electrophysiologically characterized and fully reconstructed normal (TDL and somatic area, $n = 11$) and axotomized (TDL, $n = 11$; somatic area, $n = 13$) MNs. Figure 10*G* shows that there was a negative correlation between the MN somatic area and the input resistance in control TA MNs ($r = -0.70$,

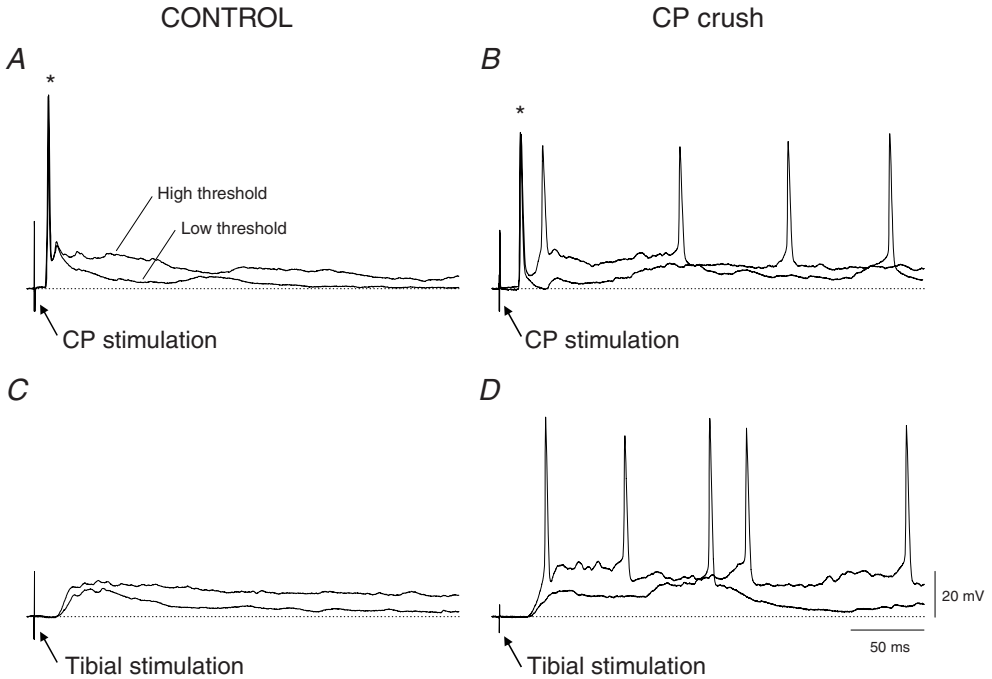

Figure 9. Enhanced synaptic responses in axotomized motoneurones
Superimposed responses evoked by low- (2 × threshold) and high-intensity stimulation (5 × threshold) from the CP nerve (*A* and *B*) and tibial nerve (*C* and *D*) in a P7 normal (*A* and *C*) and a P5 axotomized TA motoneurone (*B* and *D*). Antidromic action potentials (*) were evoked following CP nerve stimulation. Orthodromic spikes, however, were elicited only in the injured motoneurone, at low- and high-intensity stimulation from both nerves. This higher excitability in the injured motoneurone could be due to its altered passive membrane properties (resting potential, −66.1 mV; R_{in}, 12.31 MΩ; and I_{Rh} (rheobasic current) 2.02 nA) compared with the normal cell (resting potential, −61.5 mV; R_{in}, 4.02 MΩ; I_{Rh}, 4.17 nA).

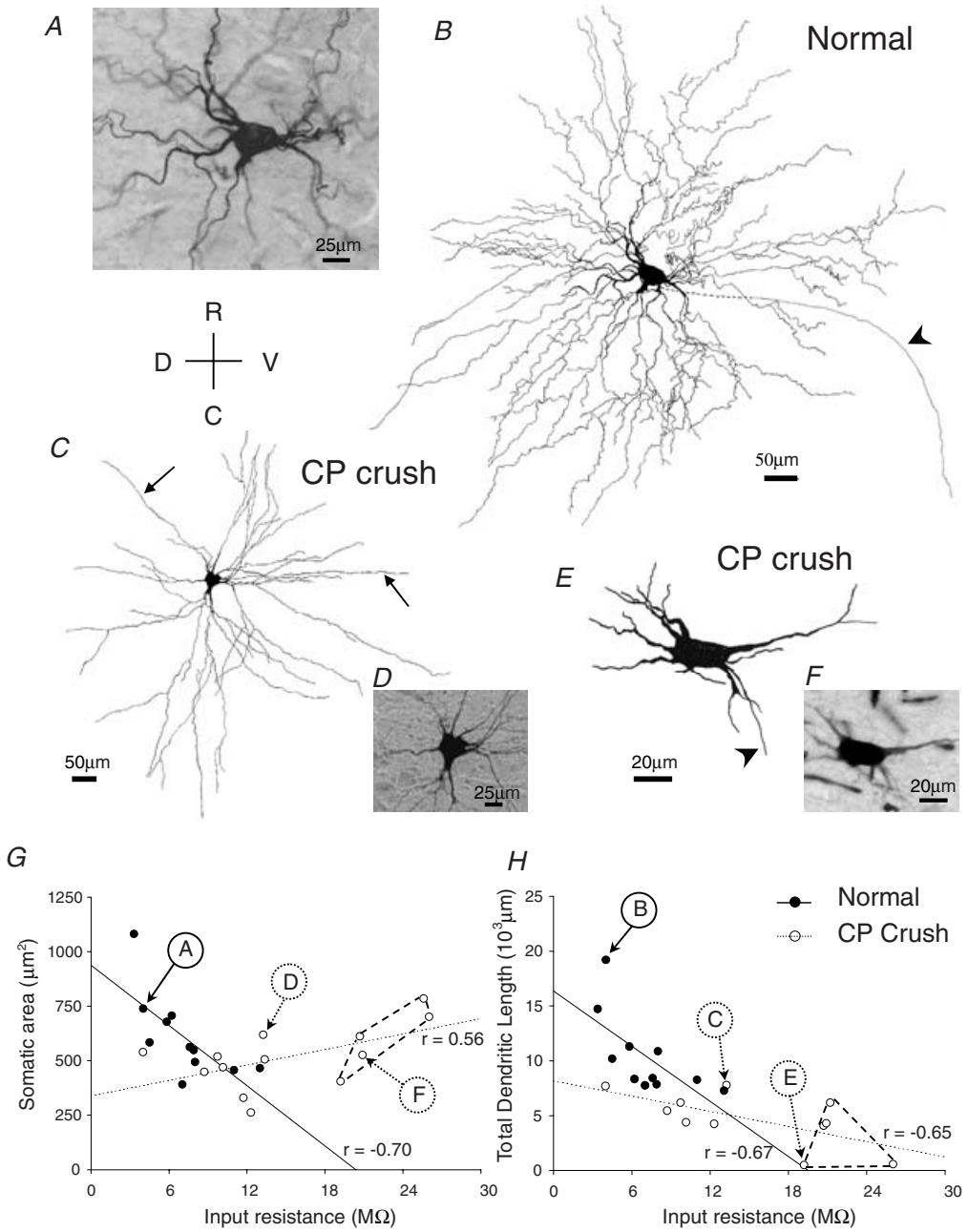

Figure 10. Marked changes in morphology of injured motoneurones and correlations with input resistance

Camera lucida reconstructions of neurobiotin-filled TA motoneurones following electrophysiological recording. A normal P7 motoneurone (*A* and *B*) and two injured MNs (P7, *C* and *D*; and P6, *E* and *F*) are shown. The photographs were taken from 100 μm thick sections. Camera lucida drawings (*B*, *C* and *E*) were constructed from all consecutive sections containing the dendritic tree. The normal motoneurone revealed an extensive and elaborate dendritic tree (*B*). In contrast, injured motoneurones revealed a less extensive dendritic tree (C and *E*). Some injured motoneurones possessed dendrites with fewer branching points (arrows in *C* point to unbranched dendrites). A small number of injured motoneurones exhibited gross hypotrophy of dendrites (*E*). In some motoneurones, the axon was visible (arrowhead in *B* and *E*). Correlations between the somatic area and the input resistance (*G*) and between the total dendritic length (TDL) and the input resistance (*H*) are shown for all ages (P3–P9). Normal motoneurones showed a negative correlation between input resistance and soma size. In contrast, injured cells showed a significant positive correlation. The TDL in normal motoneurones was negatively correlated with their corresponding input resistance. Although injured motoneurones revealed a dendritic tree of smaller extent, this was also negatively correlated with their input resistance. Dashed lines highlight the subpopulation of injured motoneurones with abnormally high values of input resistance. The positions of the normal and injured cells (normal, *A* and *B*; injured, *C*—*F*) are appropriately marked in the graphs.

$P = 0.01$, Pearson product–moment correlation), whereas a positive correlation was observed for injured TA motoneurones ($r = 0.59$, $P = 0.04$, Pearson product–moment correlation). In addition, there was a negative correlation between input resistance and TDL (Fig. 10*H*) for both normal ($r = -0.67$, $P = 0.02$, Pearson product–moment correlation, $n = 11$) and injured MNs ($r = -0.65$, $P = 0.03$, Pearson product–moment correlation, $n = 11$) which was not statistically different ($P > 0.05$, difference test for r) when compared with that of the normal MNs. Interestingly, the subset of injured TA motoneurones (∼45%, 5/11) which exhibited abnormally high input resistance (i.e. higher than the any of the control cells) corresponded to those cells that showed the smallest TDL compared with any of the control cells (Fig. 10*H*). This subset of injured MNs may therefore represent a state of neurodegeneration just prior to cell death.

Discussion

We show here that the excitability and firing patterns of MNs are profoundly altered shortly after neonatal axotomy, at a time when a significant proportion of the cells are degenerating while the remainder are in the process of reinnervating their target muscle. We found that motoneurone excitability was increased, as indicated by changes in passive and active membrane electrical properties. These changes were associated with a shift in the firing pattern of the motoneurones from a predominantly phasic pattern to a tonic pattern.

The most severe alterations in some of the electrophysiological properties were associated with presumptive morphological signs of degeneration, such as a severely reduced dendritic tree, suggesting that excessive neuronal excitability may be accompanied by cell death. About 75% of TA MNs are lost during the first 3 weeks following neonatal axotomy. The peak rate of death occurred within the first week postinjury, which is in accordance with studies showing that neonatal axotomy results in massive MN death (Schmalbruch, 1984; Lowrie *et al.* 1987).

Passive membrane properties and morphological alterations

The R_{in} and time constant of normal TA MNs decreased during development while the rheobasic current increased, which is consistent with previous reports in spinal and hypoglossal MNs (Fulton & Walton, 1986; Núñez-Abades *et al.* 1993; Viana *et al.* 1993*b*; Vinay *et al.* 2000). Axotomized MNs, however, exhibited increased R_{in} and time constant while the rheobase current decreased. It is generally accepted that the R_{in} increases following adult axotomy (Kuno *et al.* 1974; Gustafsson & Pinter, 1984; Sernagor *et al.* 1986) although the extent of this alteration depends on MN type (Titmus & Faber, 1990).

In this study, ∼30% of TA motoneurones showed disproportionately high values of R_{in}, similar to those reported for axotomized neonatal facial MNs (Umemiya *et al.* 1993). Correlations of R_{in} with morphological characteristics of the axotomized cells revealed that those cells that showed the most severe alteration in cell excitability also had the most severe reductions in TDL, while showing only moderate changes in somatic area. Furthermore, axotomized MNs possessed dendrites with fewer dendritic branches compared with normal MNs. In a few cases, morphological abnormalities, such as swelling of proximal dendrites and varicosities in distal dendrites, were observed (data not shown), which have been seen in advanced stages of degeneration (Barron, 1975). It is therefore unlikely that the increase in R_{in} could simply be accounted for by alterations in somatic size, as suggested by Laiwand *et al.* (1988) in degenerating vagal neurones. Thus, it is possible that other factors, such as changes in specific membrane resistance, as reported in axotomized corticospinal neurones (Tseng & Prince, 1996), could contribute to changes in passive membrane properties.

Action potential characteristics

In normal MNs, the rising phase of the AP was characterized by a clear break between the initial segment and the somatodendritic component (Brock *et al.* 1953). In contrast, axotomized MNs did not display a clear IS-SD break, and the rate of rise of the AP was significantly faster. These changes may be due to an upregulation of functional voltage-sensitive Na^+ channels in the somatodendritic compartment, as demonstrated in axotomized crayfish neurones (Kuwada, 1981). Injury of adult cat MN axons results in abnormal excitability of the somatodendritic membrane, characterized by the presence of partial spikes (Eccles *et al.* 1958; Kuno & Llinás, 1970), which are Na^+ dependent (Sernagor *et al.* 1986). The increased amplitude and overshoot of the AP found in injured MNs argues further for an increase in membrane excitability, which may be attributed to an enhanced synthesis and insertion of Na^+ channels in regions outside the initial segment, as suggested by Kuno & Llinás (1970). Recent results showing an increase in persistent Na^+ currents in MNs from transgenic animals expressing an SOD1 (superoxide dismutase 1) mutation present in familial forms of human amyotrophic lateral sclerosis (Kuo *et al.* 2005) suggest that changes in Na^+-dependent excitability may be an important factor in determining MN vulnerability to neurodegeneration.

Neonatal MNs exhibit a prominent ADP, which is associated with voltage-activated calcium conductances (Walton & Fulton, 1986; Viana *et al.* 1993*a*; Gao & Ziskind-Conhaim, 1998; Martin-Caraballo & Greer, 2001; Miles *et al.* 2004) activated during the repolarizing phase of the AP. In this study, the presence of ADP in normal

TA MNs was also associated with a high incidence of 'doublet' or burst firing, with the second spike riding on the ADP as previously reported (Navarrete & Walton, 1989; Viana *et al.* 1993*a*). Following injury, the incidence of both the ADP and doublet firing was markedly decreased. Since an analysis of the various ionic conductances was not attempted in this study, is not possible to state with certainty which calcium conductances are differentially affected by axotomy. However, it is interesting that, in organotypic cultures of adult turtle spinal cord where MNs are deprived of contact with their target muscle, there is a selective reduction of L-type calcium conductances which are normally found in the soma, proximal and distal dendrites (Simon *et al.* 2003). This change was associated with a reduction of the dendritic tree, an observation also made in the present study.

In our study, axotomized neonatal TA motoneurones showed a significant increase in the amplitude and duration of the AHP. Furthermore, a subpopulation of ∼35% of injured MNs exhibited longer AHP durations than the longest AHP recorded in control MNs. Since axotomy of neonatal facial MNs has been shown to have no significant effect on calcium-activated potassium conductances (Umemiya *et al.* 1993) it is possible that these changes may be secondary to changes in calcium conductances. It has been shown that the AHP is dependent on calcium-activated potassium currents (Walton & Fulton, 1986; Viana *et al.* 1993*a*,*b*; Martin-Caraballo & Greer, 2001). It is thought that the main calcium channels affecting the AHP are the N-type Ca^{2+} channels (Gao & Ziskind-Conhaim, 1998; Martin-Caraballo & Greer, 2001). It is plausible, therefore, that neonatal axotomy may result in a decrease in the L-type current (leading to ADP reduction) while enhancing the N-type current (resulting in an increase of AHP). In addition, Safronov & Vogel (1996) have demonstrated that rat spinal MN somata possess sodium-activated potassium channels. Although these channels may not make any contribution to a single AP in normal animals, they may be recruited in axotomized MNs which exhibit an upregulation of sodium channels as we suggest here.

Repetitive firing

The alterations in the ADP and AHP discussed above appear to be closely linked to changes in the MN firing patterns following neonatal axotomy. The major effect was a shift in the firing pattern from predominant burst firing in normal cells to tonic firing in axotomized MNs (Table 2). Axotomized MNs also required a significantly smaller rheobasic current, another indication of the increased excitability of the injured cells. The burst firing in normal cells was associated with the presence of a prominent ADP. Some control cells (burst/tonic type only) exhibited adaptation, whereas almost all axotomized MNs (16/17) fired tonically with little or no adaptation (Fig. 8 and Table 2), probably due to the reduction in ADP and increase in AHP duration.

Our results therefore suggest that synaptic contact between the MN and its target muscle during a critical neonatal period is important in regulating the maturation of MN functional characteristics. We have previously shown that the *in vivo* firing pattern of ankle flexor MNs (such as TA) which survive neonatal sciatic nerve injury and reinnervate their target muscles is shifted towards a tonic pattern (Navarrete & Vrbová, 1984; Vejsada *et al.* 1991). The present results also indicate that early alterations in intrinsic electrophysiological properties following neonatal axotomy can lead to long-lasting changes in MN function.

Differences in synaptic activation

Although detailed analysis of synaptic potentials was not performed here, all axotomized MNs could be activated synaptically from peripheral nerves (Fig. 9) and this activation was blocked by glutamate receptor antagonists (data not shown), as shown for normal MNs (Evans & Long, 1989; Pinco & Lev-Tov, 1993). Some of the injured MNs exhibited unusually robust synaptic activation following nerve stimulation (Fig. 9). It is possible that these enhanced synaptic potentials are due to their higher intrinsic MN excitability and may compensate for the loss of monosynaptic inputs resulting from the cell death of primary afferents following neonatal nerve injury (Himes & Tessler, 1989; Dekkers *et al.* 2002). The fact that enhanced polysynaptic reflex responses are recorded from ankle dorsiflexor MNs that survive neonatal axotomy and reinnervate their target muscle (Navarrete & Vrbova, 1984; Vejsada *et al.* 1991) also suggests that a possible source of the increased synaptic drive may come from premotor interneurones, which sprout to cover the synaptic territory vacated by the primary afferents that were lost after neonatal injury. Whatever the mechanism, the increased synaptic activation of axotomized MNs may lead to a greater influx of calcium into the cell.

Comparison between neonatal and adult axotomy

The effects of adult axotomy on the intrinsic properties of motoneurones have been well studied (Eccles *et al.* 1958; Gustafsson & Pinter, 1984; Foehring *et al.* 1986). It is also known that different types of adult spinal MNs respond differently to axotomy (Kuno *et al.* 1974; reviewed by Titmus & Faber, 1990). In general, following adult axotomy, spinal motoneurones increase their input resistance and membrane time constant, the rheobase current decreases, their soma size decreases and some alterations in the dendritic geometry are observed. These changes are temporary and are thought to be dependent

upon successful reinnervation of the motoneurone with its target muscle (Foehring *et al.* 1986).

The effects of neonatal axotomy, in contrast, are less well understood. The most significant difference between neonatal and adult axotomy is that disconnection of motoneurones from their target muscles during early development leads to a massive death of motoneurones, something that is not observed after adult axotomy (except ventral root avulsion). The neonatal axotomy-induced motoneurone death is different from the programmed cell death that is observed in motoneurones during embryonic development (see review by Houenou *et al.* 1994) and is believed to be a mixed response comprising necrosis and apoptosis.

Following neonatal axotomy, we observed changes in the intrinsic properties and the firing pattern of TA motoneurones approximately 1 day after axotomy. Although we did not record from reinnervated axotomized TA motoneurones, it is possible that the altered changes in the physiological parameters of TA motoneurones reported here may be permanent. This suggestion is in accordance with the proposal that motoneurones following axotomy may revert to a dedifferentiated status and therefore fire as slow-twitch motoneurones (i.e. soleus motoneurones; Gustafsson & Pinter, 1984). Functional differentiation into distinct slow and fast motoneurone types occurs during the first two postnatal weeks in the rat (Navarrete & Vrbová, 1983). The input resistance of TA and EDL motoneurones, for example, decreases within the first 2 weeks after birth, resulting in an overall reduction in motoneurone excitability. This process may be halted by neonatal axotomy and consequently the TA motoneurones may remain highly susceptible to discharge.

Factors involved in motoneurone vulnerability after neonatal axotomy

In this study, we recorded from axotomized MNs that may degenerate or successfully reinnervate and survive to adulthood. It is not known which electrophysiological parameters are associated with degeneration and which reflect regenerative processes. It is possible that the subpopulation of MNs exhibiting extreme alterations in membrane excitability may represent MNs destined to die (prelethal stage), as proposed by Umemiya *et al.* (1993) for axotomized facial MNs. Indeed, a virtually complete retraction of the dendritic tree was observed in those TA MNs showing the largest increase in input resistance (Fig. 10). We postulate that the early alterations in passive and active membrane electrical properties following axotomy reported here may increase the vulnerability of MNs to cell death. It is possible that alteration in a range of ionic conductances discussed above could lead to pathological changes in intracellular calcium (Yarom *et al.* 1985) and activation of degradative processes, such as mitochondrial dysfunction and caspase activation (for review see Orrenius *et al.* 2003) leading to excitotoxic cell death (Choi, 1992; Carriedo *et al.* 1996; Martin *et al.* 1998). This proposal is consistent with the finding that blockade of glutamate receptors markedly reduces the extent of neonatal axotomy-induced cell death (Mentis *et al.* 1993).

References

Barron KD (1975). Ultrastructural changes in dendrites of central neurons during axon reaction. *Adv Neurol* **12**, 384–397.

Brock LG, Coombs JS & Eccles JC (1953). Intracellular recording from antidromically activated motoneurones. *J Physiol* **122**, 429–461.

Carriedo SG, Yin HZ & Weiss JH (1996). Motor neurons are selectively vulnerable to AMPA/kainate receptor-mediated injury *in vitro*. *J Neurosci* **16**, 4069–4079.

Choi DW (1992). Excitotoxic cell death. *J Neurobiol* **23**, 1261–1276.

Dekkers J, Becker DL, Cook JE & Navarrete R (1994). Early postnatal changes in the somatodendritic morphology of ankle flexor motoneurones in the rat. *Eur J Neurosci* **6**, 87–97.

Dekkers J, Greensmith L & Navarrete R (2002). Changes in the expression of parvalbumin immunoreactivity in the lumbar spinal cord of the rat following neonatal nerve injury. *Dev Neurosci* **24**, 283–293.

Dekkers J & Navarrete R (1998). Persistence of somatic and dendritic growth associated processes and induction of dendritic sprouting in motoneurones after neonatal axotomy in the rat. *Neuroreport* **9**, 1523–1527.

Eccles JC, Libet B & Young RR (1958). The behavior of chromatolysed motoneurones studied by intracellular recording. *J Physiol* **143**, 11–40.

Evans RH & Long SK (1989). Primary afferent depolarization in the rat spinal cord is mediated by pathways utilising NMDA and non-NMDA receptors. *Neurosci Lett* **100**, 231–236.

Foehring RC, Sypert GW & Munson JB (1986). Properties of self-reinnervated motor units of medial gastrocnemius of cat. II. Axotomized motoneurons and time course of recovery. *J Neurophysiol* **55**, 947–965.

Fulton BP & Walton KD (1986). Electrophysiological properties of neonatal rat motoneurones studied *in vitro*. *J Physiol* **370**, 651–678.

Gao B-X & Ziskind-Conhaim L (1998). Development of ionic currents underlying changes in action potential waveforms in rat spinal motoneurons. *J Neurophysiol* **80**, 3047–3061.

Gougoulias N, Kouvelas D & Albani M (2007). Protective effect of PNQX on motor units and muscle property after sciatic nerve crush in neonatal rats. *Pharmacol Res* 55, 370–377.

Greensmith L, Mentis GZ & Vrbova G (1994). Blockade of *N*-methyl-D-aspartate receptors by MK-801 (dizocilpine maleate) rescues motoneurones in developing rats. *Brain Res Dev Brain Res* **81**, 162–170.

Greensmith L & Navarrete R (1994). Effect of neonatal nerve injury on the expression of major histocompatibility complex antigens in the rat spinal cord. *Neurodegeneration* **3**, 235–242.

Greensmith L, Sanusi J, Mentis GZ & Vrbova G (1995). Transient muscle paralysis in neonatal rats renders motoneurons susceptible to *N*-methyl-D-aspartate-induced neurotoxicity. *Neuroscience* **64**, 109–115.

Gustafsson B & Pinter MJ (1984). Effects of axotomy on the distribution of passive electrical properties of cat motoneurons. *J Physiol* **356**, 433–442.

Himes BT & Tessler A (1989). Death of some dorsal root ganglion neurons and plasticity of others following sciatic nerve section in adult and neonatal rats. *J Comp Neurol* **284**, 215–230.

Horikawa K & Armstrong WE (1988). A versatile means of intracellular labeling: injection of biocytin and its detection with avidin conjugates. *J Neurosci Meth* **25**, 1–11.

Houenou LJ, Li L, Lo AC, Yan Q & Oppenheim RW (1994). Naturally occurring and axotomy-induced motoneuron death and its prevention by neurotrophic agents: a comparison between chick and mouse. *Prog Brain Res* **102**, 217–226.

Kashihara Y, Kuno M & Miyata Y (1987). Cell death of axotomized motoneurones in neonatal rats, and its prevention by peripheral reinnervation. *J Physiol* **386**, 135–148.

Kudo N & Yamada T (1987). Morphological and physiological studies of development of the monosynaptic reflex pathway in the rat lumbar spinal cord. *J Physiol* **389**, 441–459.

Kuno M & Llinás R (1970). Enhancement of synaptic transmission by dendritic potentials in chromatolysed motoneurones of the cat. *J Physiol* **210**, 807–821.

Kuno M, Miyata Y & Muñoz-Martínez EJ (1974). Differential reaction of fast and slow α-motoneurones to axotomy. *J Physiol* **240**, 725–739.

Kuo JJ, Siddique T, Fu R & Heckman CJ (2005). Increased persistent Na^+ current and its effect on excitability in motoneurones cultured from mutant SOD1 mice. *J Physiol* **563**, 843–854.

Kuwada JY (1981). Ionic and metabolic dependence of axotomy-induced somatic membrane changes in crayfish. *J Physiol* **317**, 463–473.

Laiwand R, Werman R & Yarom Y (1988). Electrophysiology of degenerating neurones in the vagal motor nucleus of the guinea-pig following axotomy. *J Physiol* **404**, 749–766.

Lowrie MB, Krishnan S & Vrbová G (1987). Permanent changes in muscle and motoneurones induced by nerve injury during a critical period of development of the rat. *Dev Brain Res* **310**, 91–101.

Lowrie MB & Vrbová G (1992). Dependence of postnatal motoneurones on their targets: review and hypothesis. *Trends Neurosci* **15**, 80–84.

Martin LJ, Al-Abdulla NA, Brambrink AM, Kirsch JR, Sieber FE & Portera-Cailliau C (1998). Neurodegeneration in excitotoxicity, global cerebral ischemia, and target deprivation: a perspective on the contributions of apoptosis and necrosis. *Brain Res Bull* **46**, 281–309.

Martin-Caraballo M & Greer JJ (2001). Voltage-sensitive calcium currents and their role in regulating phrenic motoneuron electrical excitability during the perinatal period. *J Neurobiol* **46**, 231–248.

Mentis GZ, Greensmith L & Vrbova G (1993). Motoneurons destined to die are rescued by blocking *N*-methyl-D-aspartate receptors by MK-801. *Neuroscience* **54**, 283–285.

Miles GB, Lipski J, Lorier AR, Laslo P & Funk GD (2004). Differential expression of voltage-activated calcium channels in III and XII motoneurones during development in the rat. *Eur J Neurosci* **20**, 903–913.

Naidu MDK, Subramaniam K & Vrbová G (1996). Re-innervation of muscles after nerve injury in neonates. *Rest Neurol Neurosci* **10**, 35–42.

Navarrete R (1991). Early changes in motoneurone synaptic activation recorded *in vitro* following neonatal nerve injury in the rat. *J Physiol* **438**, 220*P*.

Navarrete R & Vrbová G (1983). Changes of activity patterns in slow and fast muscles during postnatal development. *Devl Brain Res* **8**, 11–19.

Navarrete R & Vrbová G (1984). Differential effect of nerve injury at birth on the activity pattern of reinnervated slow and fast muscles of the rat. *J Physiol* **351**, 675–685.

Navarrete R & Walton KD (1989). Calcium conductances trigger doublet firing in neonatal rat motoneurones *in vitro*. *J Physiol* **415**, 70*P*.

Núñez-Abades PA, Spielmann JM, Barrionuevo G & Cameron WE (1993). In vitro electrophysiology of developing genioglossal motoneurons in the rat. *J Neurophysiol* **70**, 1401–1411.

Orrenius S, Zhivotovsky B & Nicotera P (2003). Regulation of cell death: the calcium-apoptosis link. *Nat Rev Mol Cell Biol* **4**, 552–565.

Peyronnard JM & Charron L (1983). Motoneuronal and motor axonal innervation in the rat hindlimb: a comparative study using horseradish peroxidase. *Exp Brain Res* **50**, 125–132.

Peyronnard JM, Charron L, Lavoie J & Messier JP (1986). Motor, sympathetic and sensory innervation of rat skeletal muscles. *Brain Res* **373**, 288–302.

Pinco M & Lev-Tov A (1993). Synaptic excitation of α-motoneurons by dorsal root afferents in the neonatal rat spinal cord. *J Neurophysiol* **70**, 406–417.

Romanes GJ (1946). Motor localisation and the effects of nerve injury on the ventral horn cells of the spinal cord. *J Anat* **80**, 11–131.

Safronov BV & Vogel W (1996). Properties and functions of Na^+-activated K^+ channels in the soma of rat motoneurones. *J Physiol* **497**, 727–734.

Schmalbruch H (1984). Motoneuron death after sciatic nerve section in newborn rats. *J Comp Neurol* **224**, 252–258.

Seebach BS & Ziskind-Conhaim L (1994). Formation of transient inappropriate sensorimotor synapses in developing rat spinal cords. *J Neurosci* **14**, 4520–4528.

Sernagor E, Yarom Y & Werman R (1986). Sodium-dependent regenerative responses in dendrites of axotomized motoneurons in the cat. *Proc Natl Acad Sci U S A* **83**, 7966–7970.

Simon M, Perrier JF & Hounsgaard J (2003). Subcellular distribution of L-type Ca^{2+} channels responsible for plateau potentials in motoneurons from the lumbar spinal cord of the turtle. *Eur J Neurosci* **18**, 258–266.

Titmus MJ & Faber DS (1990). Axotomy-induced alterations in the electrophysiological characteristics of neurons. *Prog Neurobiol* **35**, 1–51.

Tseng GF & Prince DA (1996). Structural and functional alterations in rat corticospinal neurons after axotomy. *J Neurophysiol* **75**, 248–267.

Umemiya M, Araki I & Kuno M (1993). Electrophysiological properties of axotomized facial motoneurones that are destined to die in neonatal rats. *J Physiol* **462**, 661–678.

Vejsada R, Hník P, Navarrete R, Palecek J, Soukup T, Borecka U & Payne R (1991). Motor functions in rat hindlimb muscles following neonatal sciatic nerve crush. *Neuroscience* **40**, 267–275.

Viana F, Bayliss DA & Berger AJ (1993*a*). Calcium conductances and their role in the firing behavior of neonatal rat hypoglossal motoneurons. *J Neurophysiol* **69**, 2137–2149.

Viana F, Bayliss DA & Berger AJ (1993*b*). Multiple potassium conductances and their role in action potential repolarization and repetitive firing behavior of neonatal rat hypoglossal motoneurons. *J Neurophysiol* **69**, 2150–2163.

Vinay L, Brocard F & Clarac F (2000). Differential maturation of motoneurons innervating ankle flexor and extensor muscles in the neonatal rat. *Eur J Neurosci* **12**, 4562–4566.

Virgo L, Dekkers J, Mentis GZ, Navarrete R & de Belleroche J (2000). Changes in expression of NMDA receptor subunits in the rat lumbar spinal cord following neonatal nerve injury. *Neuropathol Appl Neurobiol* **26**, 258–272.

Walton KD & Fulton BP (1986). Ionic mechanisms underlying the firing properties of rat neonatal motoneurons. *Neuroscience* **19**, 669–683.

Walton KD & Navarrete R (1991). Postnatal changes in motoneurone electrotonic coupling studied in the *in vitro* rat spinal cord. *J Physiol* **433**, 283–305.

Wiese S, Beck M, Karch C & Sendtner M (2004). Signalling mechanisms for survival of lesioned motoneurons. *Acta Neurochir* **89**, 21–35.

Yarom Y, Sugimori M & Llinás R (1985). Ionic currents and firing patterns of mammalian vagal motoneurons in vitro. *Neuroscience* **16**, 719–737.

Ziskind-Conhaim L (1990). NMDA receptors mediate poly- and monosynaptic potentials in motoneurons of rat embryos. *J Neurosci* **10**, 125–135.

Acknowledgements

The authors would like to thank Drs. R. Burke, M. J. O'Donovan, A. Pastor and R. de la Cruz for helpful comments on the manuscript. This work was supported by the Wellcome Trust (038962 to R. N.), the European Union (B104-96-0649 to R. N.) and in part by the Intramural Research Program of the NIH, NINDS (to G.Z.M.).

Authors' present addresses

E. Díaz: Program of Anatomy and Developmental Biology, Institute of Biomedical Sciences, Faculty of Medicine, University of Chile, Correo 7, Santiago, 6530499, Chile.

L. B. Moran: University Department of Neuropathology, Division of Neuroscience and Mental Health, Faculty of Medicine, Imperial College London, London, UK.